The following States are Members of the International Atomic Energy Agency:

AFGHANISTAN
ALBANIA
ALGERIA
ARGENTINA
ARMENIA
AUSTRALIA
AUSTRIA
BANGLADESH
BELARUS
BELGIUM
BOLIVIA
BRAZIL
BULGARIA
CAMBODIA
CAMEROON
CANADA
CHILE
CHINA
COLOMBIA
COSTA RICA
COTE D'IVOIRE
CROATIA
CUBA
CYPRUS
CZECH REPUBLIC
DENMARK
DOMINICAN REPUBLIC
ECUADOR
EGYPT
EL SALVADOR
ESTONIA
ETHIOPIA
FINLAND
FRANCE
GABON
GERMANY
GHANA
GREECE
GUATEMALA
HAITI
HOLY SEE
HUNGARY
ICELAND
INDIA
INDONESIA
IRAN, ISLAMIC REPUBLIC OF
IRAQ
IRELAND
ISRAEL
ITALY
JAMAICA
JAPAN
JORDAN
KAZAKHSTAN
KENYA
KOREA, REPUBLIC OF
KUWAIT
LEBANON
LIBERIA
LIBYAN ARAB JAMAHIRIYA
LIECHTENSTEIN
LITHUANIA
LUXEMBOURG
MADAGASCAR
MALAYSIA
MALI
MARSHALL ISLANDS
MAURITIUS
MEXICO
MONACO
MONGOLIA
MOROCCO
MYANMAR
NAMIBIA
NETHERLANDS
NEW ZEALAND
NICARAGUA
NIGER
NIGERIA
NORWAY
PAKISTAN
PANAMA
PARAGUAY
PERU
PHILIPPINES
POLAND
PORTUGAL
QATAR
ROMANIA
RUSSIAN FEDERATION
SAUDI ARABIA
SENEGAL
SIERRA LEONE
SINGAPORE
SLOVAKIA
SLOVENIA
SOUTH AFRICA
SPAIN
SRI LANKA
SUDAN
SWEDEN
SWITZERLAND
SYRIAN ARAB REPUBLIC
THAILAND
THE FORMER YUGOSLAV REPUBLIC OF MACEDONIA
TUNISIA
TURKEY
UGANDA
UKRAINE
UNITED ARAB EMIRATES
UNITED KINGDOM OF GREAT BRITAIN AND NORTHERN IRELAND
UNITED REPUBLIC OF TANZANIA
UNITED STATES OF AMERICA
URUGUAY
UZBEKISTAN
VENEZUELA
VIET NAM
YEMEN
YUGOSLAVIA
ZAIRE
ZAMBIA
ZIMBABWE

The Agency's Statute was approved on 23 October 1956 by the Conference on the Statute of the IAEA held at United Nations Headquarters, New York; it entered into force on 29 July 1957. The Headquarters of the Agency are situated in Vienna. Its principal objective is "to accelerate and enlarge the contribution of atomic energy to peace, health and prosperity throughout the world".

Printed by the IAEA in Austria
March 1995
STI/PUB/944

ENERGY FROM INERTIAL FUSION

INTERNATIONAL ATOMIC ENERGY AGENCY
VIENNA, 1995

SECTION 1: Pgs. 2 - 5

In inertial confinement fusion (ICF), a driver (usually either a laser or a particle accelerator) delivers an intense pulse of energy to a target consisting of a small capsule of DT fuel and other surrounding structures that are needed to ensure adequate target performance. The energy is delivered in such a way as to cause the fuel capsule to implode, creating very high densities in the main fuel and very high temperatures in a small, central fraction of that fuel (called the hot spot or spark plug). The thermonuclear reactions in the hot spot release energetic neutrons and charged particles. The charged particles deposit their energy in the inner layer of the surrounding cold fuel, heating and igniting it, thereby causing a thermonuclear burn front to propagate outward through the rest of the cold, compressed fuel. The thermonuclear burn front travels through the fuel in a time that is shorter than the time it takes for the compressed target to fly apart. If more energy is produced in this fusion 'pulse' than was delivered to the target, it is said that the target has a gain greater than one. Chapter 2 of this book will describe the physical processes occurring inside the target in more detail.

In an inertial fusion energy (IFE) power plant, the thermonuclear energy pulses occur a few times per second. The energy released in each pulse is 100–1000 MJ, or the chemical equivalent of 25–250 kg of high explosive. The energy appears as rapidly moving neutrons, a large flux of X rays and a rapidly expanding cloud of plasma (called debris). The debris is composed of the leftover fusion fuel, the fusion products and the other materials that were used to make the target. These materials

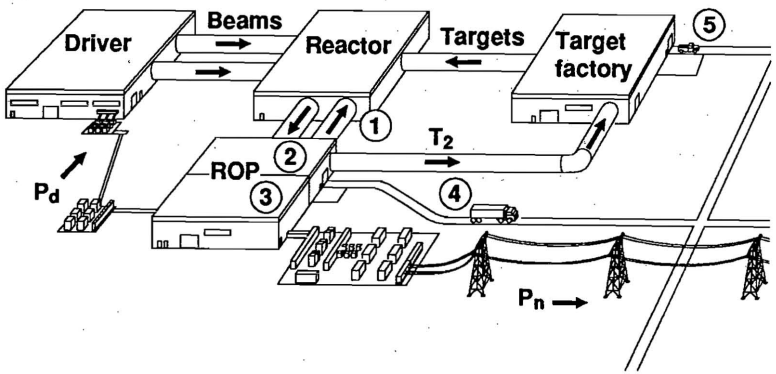

FIG. 1.1. An IFE power plant consists of four almost, but not completely, independent systems: the driver, the target factory, the reactor and the remainder of plant (ROP). Blanket material flows between the reactor and the ROP (1), transporting heat and T_2. In the ROP the T_2 and other target materials are extracted (2) and sent to the target factory. Electricity is generated (3) to supply the grid and the driver. Waste is processed and shipped off-site (4). D_2 and Li are delivered (5) for replacing burned fuel and transmuted blanket material. (P_d: driver power; P_n: net power.)

are at such a high temperature as to be ionized and form a plasma. The energy of these emissions must be captured in the reactor and potential adverse effects contained. The thermonuclear energy pulses are converted to thermal energy in order to produce a steady electric power source. This process is analogous to that of the internal combustion engine, in which a rapid succession of tiny chemical explosions is converted to mechanical energy to run an automobile.

In an IFE power plant, targets must be manufactured, filled with fuel and supplied to the reactor at the rate of a few per second. Tritium, one of the two components of the fuel, is radioactive and has a limited lifetime. It must be manufactured in the reactor or elsewhere and supplied to the target factory. The initial amount of tritium needed is brought from a fission reactor or another fusion power plant. Once the plant is in operation, tritium can be manufactured by exposing lithium to the neutrons produced in the reactor. A nuclear reaction between lithium and neutrons produces tritium in addition to helium, a benign by-product, and also releases further nuclear energy. Thus, the fuel routinely brought into a fusion power plant actually consists of deuterium and lithium (neither is radioactive).

An IFE power plant consists of four major, separate but interconnected systems (Fig. 1.1):

(a) The driver, usually either a laser or a particle accelerator, converts electrical power into short pulses of light or particles and delivers them to the ICF target in the proper spatial and temporal form to cause implosion, ignition and thermonuclear burn, i.e. fusion.

(b) In the target factory, targets are manufactured, filled with DT fuel and sent to the reactor. The deuterium comes from outside the plant while the tritium is manufactured in the reactor.

(c) In the reactor, targets are sequentially injected into a reaction chamber and tracked, i.e. their position and orientation are precisely measured. Driver beams are directed to the target to produce thermonuclear pulses a few times a second. The thermonuclear emissions are captured in a surrounding structure called a blanket and their energy is converted into thermal energy (heat). (In some power plant designs a portion of the thermonuclear energy is directly converted into electricity.) Tritium is also produced in the blanket.

(d) In the remainder of plant (ROP), two major processes are performed. Tritium and some other target materials are extracted from the recirculating blanket material and from the reaction chamber exhaust gases. Then these extracted materials are recycled to the target factory. Thermal energy is converted into electricity, a portion of which is conditioned and recirculated to power the driver. Lithium from outside the plant is processed and supplied to the reaction chamber to replace that used to make tritium.

The systems conceived to carry out all these functions are described in detail in Chapter 3. Three very important design issues are described in greater depth in

Chapter 4: these are the lifetime of structural materials in a pulsed radiation environment, neutron activation of materials and the structural interfaces between the driver and the reactor.

In an IFE power plant, there are two major cycles to consider: the power cycle and the target materials cycle. In the power cycle, a series of energy conversion processes occurs, each with a characteristic efficiency. Electrical energy is converted to light or particle beam energy in the driver with an efficiency η. That energy is converted into thermonuclear energy by the target with a gain G. The thermonuclear energy is converted into thermal energy in the blanket inside the reaction chamber and increased by a factor M through the neutron reactions. Finally, the heat energy is converted to electricity in the ROP with an efficiency ϵ. A portion of the gross electricity produced must be recirculated to power the driver, completing the power cycle.

In the target materials cycle, complete targets disintegrate in the reactor and a portion of the DT fuel is burned. Target debris is deposited in the chamber gas and/or in the blanket material. Tritium fuel is manufactured in the blanket. The tritium and other target materials are extracted, conditioned and returned to the target factory for use in future targets.

Central to the economics of any IFE power plant is the power cycle gain [1.1]. A power flow diagram for an IFE power plant is shown in Fig. 1.2. The power cycle gain is the product of the driver efficiency η, the target gain G, the energy multiplier M due to reactions in the blanket, and the thermal to electric conversion

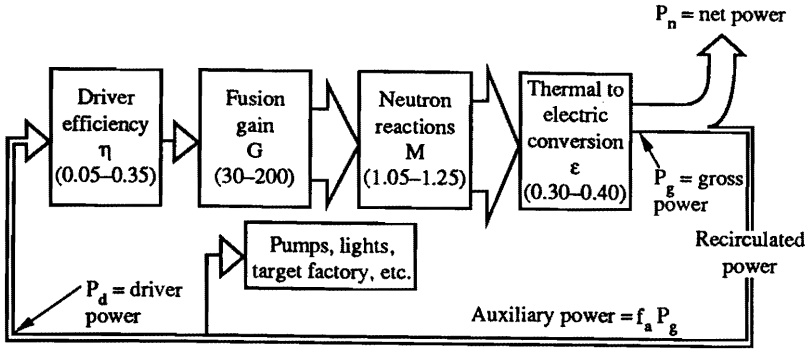

FIG. 1.2. Power in an IFE power plant is supplied to a driver where it is reduced by the driver efficiency η, enhanced by the target gain G *and blanket multiplier* M, *and reduced again by the thermal to electric conversion efficiency ϵ. Part of the gross power produced is recycled to supply the driver and auxiliary equipment.*

efficiency ϵ. In the plant, the net electricity to be distributed, P_n, is related to the gross electricity P_g through the power balance equation

$$P_n = P_g - P_a - P_d = P_g(1 - f_a - 1/\eta GM\epsilon)$$

where P_a, which is equal to $f_a P_g$, is the power used for auxiliary equipment and P_d is the power supplied to the driver. Typical values of f_a are 5%.

The equation shows that the fraction of the gross power that is recirculated to the driver, P_d/P_g, is just the inverse of the power cycle gain. While not universally true, a simple rationale can lead to a useful rule of thumb for the target gains required for competitive economics. If the recirculating power fraction is too large (e.g. $\geq$25%), then the cost of electricity sold rises rapidly because much of the plant equipment is used simply to generate electricity for the driver itself (Fig. 7.6). Thus, the power cycle gain should be greater than $\sim$4. Typically, M is about 1.05–1.25 and ϵ ranges from 30 to 40%. Therefore, for good economics, the product ηG should be greater than about 10. This product determines the minimum target gain necessary for any given driver efficiency. Driver efficiency ranges from about 5 to 35%, depending upon driver type, and therefore target gains of 30–200 will be required. Since driver cost usually increases rapidly with driver energy, it is most important to obtain the necessary gain at the lowest possible driver energy (for a given driver efficiency). Chapter 7 discusses economic issues in much more detail.

An IFE power plant is very different from present ICF research facilities. In this book, each chapter and section describing a portion of such a power plant will also describe the major development issues that must be resolved before the plant can be built. Chapter 5 will discuss various options for IFE development. It should be noted, in the power balance equation, that to reach power break-even, i.e. to produce just enough power to operate the driver, requires a power cycle gain of only 1. Thus, the minimum gain for power break-even is a factor of 4 or so smaller than that required to keep the cost of power sold reasonable. This will have important implications for the cost of developing IFE.

IFE power plants must be safe for workers and the public and must have minimum impact on the environment. Ensuring these features requires that all systems and materials needed for successful operation of such plants be examined carefully for their potential negative impacts. Chapter 6 is devoted to this very important topic.

1.2. FUTURE ENERGY REQUIREMENTS

1.2.1. Past Trends and Driving Factors for Energy Demand

Energy is fundamental to improving the conditions of life on this planet. The availability of inexpensive fossil fuels has been largely responsible for the rapid economic growth of the last two centuries. As the end of this century nears, however,

energy production using ICF, this chapter will concentrate on an overview of the important physics issues associated with ICF targets relevant to future energy producing power plant applications. Those readers interested in more details associated with the physics of ICF and its historical development are referred to Refs [2.4–2.8] and the references therein.

In Section 2.2 we shall introduce the basic concepts, followed by a more detailed discussion in Section 2.3. Section 2.3 also includes experimental results obtained throughout the ICF community on existing laboratory facilities. These facilities include laser systems at Lawrence Livermore National Laboratory (LLNL), USA (Nova); the Institute of Laser Engineering (ILE), Japan (GEKKO XII); the CEA Centre d'études de Limeil-Valenton (CEL-V), France (Phebus and Octal); the University of Rochester Laboratory for Laser Energetics (LLE), USA (Omega); and the All-Russian Research Institute of Experimental Physics, Arzamas, Russian Federation (Iskra-5). Light ion experimental results are currently being obtained at Sandia National Laboratories (SNL), USA (PBFA II). A wide variety of smaller facilities in the aforementioned countries, as well as in Germany, the United Kingdom, Italy and elsewhere, are also used for ICF research.

2.2. ICF: BASIC CONCEPTS

2.2.1. ICF Power Gain and Driver Requirements

As pointed out in Chapter 1, the thermonuclear energy released from an ICF capsule implosion in a reaction chamber is transformed into electricity, part of which is used to produce the next driver pulse in order to make the process cyclic. IFE power plant studies have shown that an economic IFE power plant will require that the product of the driver efficiency η and the thermonuclear gain G be approximately 10. The thermonuclear gain is defined as $G = E_F/E_d$ where E_F is the thermonuclear energy released from a single ICF capsule and E_d is the driver energy delivered to the reaction chamber.

Of the various possible fusion reactions, that between deuterium and tritium has the largest cross-section (Fig. 2.1) and therefore deuterium–tritium is being considered as the fuel that would be used for the first generation of IFE power plants. The reaction for DT fusion is given by

$$\underset{}{\mathrm{D} + \mathrm{T} =} \underset{14.06\ \mathrm{MeV}}{\mathrm{n}} + \underset{3.52\ \mathrm{MeV}}{\alpha}$$

(where α is ^{4}He). For DT fuel the thermonuclear energy released from a given ICF capsule can be expressed as

$$E_F = C_{DT} M_{DT} f_b$$

where C_{DT} is the specific energy of fusion (3.4×10^{11} J/g for DT), M_{DT} is the mass of the burning DT fuel and f_b is the burn fraction.

In order to achieve the requirement of $\eta G \geq 10$ at the lowest cost, as seen in Chapter 1 the goal of IFE with respect to capsule performance is to maximize the thermonuclear gain of a given ICF capsule while minimizing the driver energy. From the simple expression for the thermonuclear energy released from a given fusion pulse, maximizing the fusion output will depend on the product $M_{DT}f_b$. Therefore, in order to both minimize the size of the driver (which must increase as M_{DT} increases) and maximize the capsule output (achieve high gain) the maximization of the burn fraction is essential to the success of IFE.

2.2.2. Thermonuclear Burn Fraction

To understand what conditions are required in the imploded fuel to achieve efficient thermonuclear burn (maximize $M_{DT}f_b$), it is useful to develop a simple model for the burn fraction of DT, including the effects of depletion. The number of reactions per second is given by

$$\frac{dn_T}{dt} = -n_T n_D \langle \overline{\sigma v} \rangle$$

where $\langle \overline{\sigma v} \rangle$ is the reaction cross-section averaged over a Maxwellian distribution of particles and n_D and n_T are the particle densities of D and T. Assuming an equimolar density ($n_D = n_T$) and defining the burn fraction by

$$f_b = 1 - \frac{n}{n_0}$$

we then solve the equation for n by integrating from time $t = 0$ to the time when the capsule disassembles (confinement time), $t = \tau_d$.

In inertial confinement, the burn is quenched by hydrodynamic expansion. From the outside of the fuel, a rarefaction wave moves inward at the speed of sound, c_s. By the time this rarefaction has moved a fraction of the capsule radius R, the fuel density in most of that fuel mass has dropped significantly and the fuel in that region no longer burns efficiently [2.9]. The disassembly time is given approximately by

$$\tau_d \approx \frac{R}{4c_s}$$

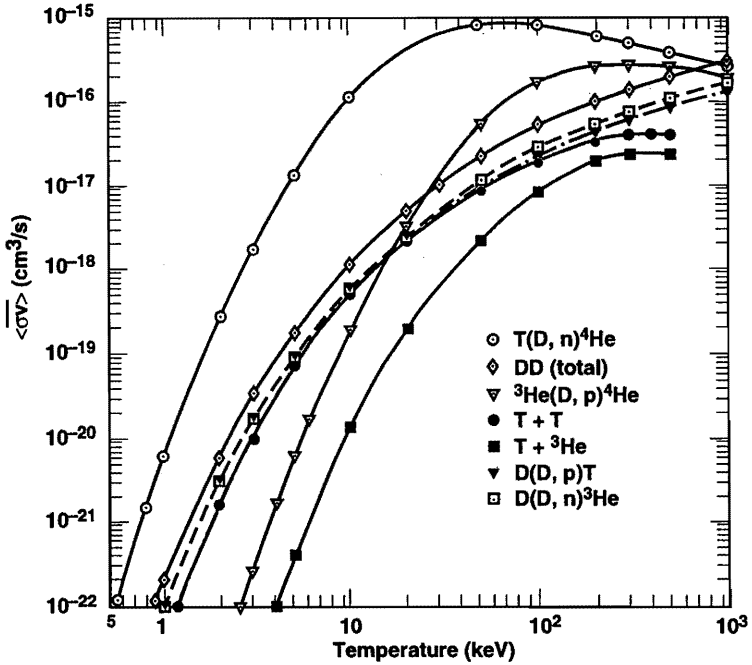

FIG. 2.1. Thermonuclear reaction rates for various fusion reactions. DT has the reaction with the largest cross-section and is therefore the fuel being considered for early ICF energy applications.

Hence, we can solve the above equation for the burn fraction, resulting in

$$f_b = \frac{\rho R}{\rho R + \xi(T)}$$

where $\xi(T) = 8m_i c_s/\langle\overline{\sigma v}\rangle$ and m_i is the mass of an ion. The quantity $\xi(T)$ is a strong function of temperature (T). Referring to Fig. 2.1, for DT between 20 and 40 keV, which represents the typical range of burn temperatures of ICF capsules, the quantity $\xi(T)$ is approximately 6 g/cm^2. The product ρR, which is generally referred to as the fuel areal density (g/cm^2), is equivalent to the $n\tau$ requirement [2.10] generally used for magnetic fusion energy (MFE). Analytic estimates as well as detailed numerical simulations have shown that a burn fraction of $\geq 30\%$ is required for gains in excess of 100, which are required for $\eta \approx 10\%$. Therefore, the value of ρR required for a high gain ICF capsule implosion is ≥ 3.0 g/cm^2.

If τ is given by τ_d, then $n\tau$ and ρR can be simply related by

$$n\tau = \frac{\rho R}{4c_s m_i}$$

The value $\rho R = 3.0$ g/cm^2 required for high gain ICF corresponds to an $n\tau$ of 2×10^{15} s/cm^3. It can be seen, therefore, that in order for ICF capsules to achieve high burn fractions, the $n\tau$ product for ICF capsules exceeds that usually quoted for MFE plasmas (10^{14} s/cm^3).

2.2.3. Implosion and Compression of Matter

As shown in the previous section, for high gain, ICF capsule implosions will require a ρR of approximately 3.0 g/cm^2. This can obviously be achieved by having either a low density, large radius configuration or a high density, small radius configuration. Simple estimates can be constructed that show that the required driver energy scales approximately as the inverse of the square of the compression of the fuel (the compression in this example being defined as $\rho_{DT}/\rho_{DT\,liq}$, where $\rho_{DT\,liq} = 0.213$ g/cm^3) [2.11]. Therefore, in order to minimize the driver size required for IFE, compression of the DT fuel will be required.

Figure 2.2 displays schematically the four important phases associated with an ICF capsule implosion, as well as an example of a radius versus time history of the imploded capsule material. Compression of the DT to high density is based on a process similar to that of the acceleration of a rocket. As the driver energy impinges on the initially solid matter of the capsule, this material is transformed into a plasma with a temperature on the order of a few kiloelectronvolts (Fig. 2.2(a)), the capsule is ablated and the heated plasma expands outward with a velocity of 100–1000 km/s. (By analogy with a rocket, the ablated material represents the burnt fuel that flows out from the rocket; however, a typical rocket velocity is only 2–3 km/s.) The plasma (burnt fuel of the rocket) gives its momentum to the remaining part of the capsule (rocket) (Fig. 2.2(b)). The remaining portion of the spherical capsule begins to move towards the centre, compressing and heating (via shocks and pressure–volume ($P\,dV$) work) the thermonuclear fuel (Fig. 2.2(c)). If, at the culmination of the implosion, specific conditions associated with the final fuel are attained [2.10], thermonuclear ignition and subsequent burnup (high gain) will occur (Fig. 2.2(d)). The relative time durations of the four important phases (Figs 2.2(a)–(d)) of an ICF capsule implosion are shown along the top of Fig. 2.2(e).

The final density attained by the fuel during a capsule implosion depends on: (1) the external driving pressure, which may reach 10^7–10^8 atm (10^{12}–10^{13} Pa); (2) the resistance of the target matter to compression; and (3) the development of hydrodynamic instabilities and asymmetry during the implosion process. The external pressure is determined by the material ablated and the incident driver energy

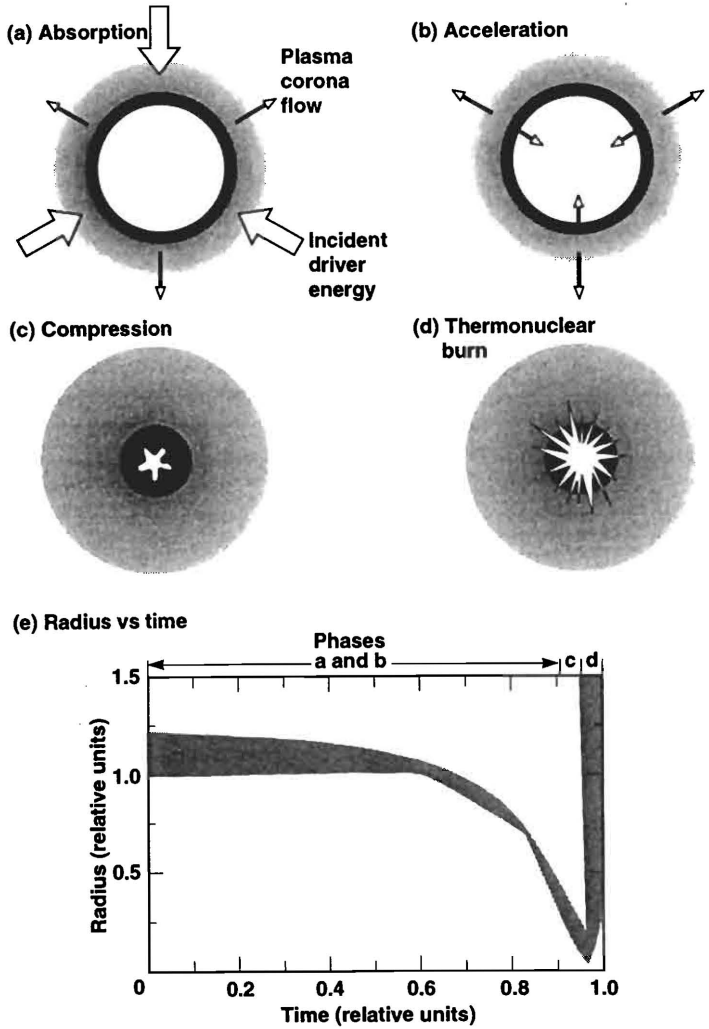

FIG. 2.2. The main phases of an ICF capsule implosion: (a) absorption of the driver energy (laser or X ray, produced by laser or ion beams) and formation of the target corona; (b) acceleration of the unablated shell material to the centre and implosion; (c) compression and heating of fuel; (d) thermonuclear burn and disassembly. (e) Radius versus time trajectory of the imploding fuel for a generic ICF capsule implosion. The time axis is in relative units where the time at the end of the thermonuclear burn phase is set to unity. The time durations of phases a–d are indicated along the upper axis.

flux. The ability to compress the material in the capsule depends on the entropy and the equation of state of the imploding material. Finally, the hydrodynamic instabilities of importance to ICF implosions are similar in nature to the classical Rayleigh–Taylor fluid instability [2.12]. There are actually two occurrences of this hydrodynamic instability during an ICF capsule implosion. The first occurs during the acceleration phase (Fig. 2.2(b)) and the second during the deceleration phase, which occurs near the end of the compression (Fig. 2.2(c)).

Symmetry requirements impose a pressure uniformity specification on the implosion. During an ICF capsule implosion, the effects of departures from spherical symmetry are most pronounced during the compression phase (Fig. 2.2(c)).

2.2.4. Ignition and Propagating Burn

For DT the energy required to heat the fuel to 10 keV is approximately 1200 MJ/g. To compress nearly Fermi-degenerate (cold) DT, the specific energy required can be expressed as $E_c = 0.35\alpha\rho_c^{2/3}$ (MJ/g), where ρ_c is the density of the cold compressed DT and α represents the degree to which the cold fuel is non-degenerate. Detailed studies have shown that the fuel densities of interest for high gain ICF applications are in the range 100–1000 g/cm^3. Therefore, the energy required to compress the fuel in a Fermi-degenerate manner is 7.5–35.0 MJ/g, substantially less than that to heat the same mass to high temperatures.

Although compression is energetically attractive and reduces the driver size required for efficient fuel burnup, high gain also requires a high temperature region (referred to as the hot spot) for ignition to occur. From these simple energy estimates, it can be seen that minimizing the amount of DT that must be incorporated in the hot spot region will be required for future IFE applications (maximum gain at minimum driver energy).

The hot spot forms during the final stages of the ICF capsule implosion. For DT fuel the capsule can be considered as transparent to the 14.06 MeV neutrons produced in the fusion reaction (especially near the time of ignition). Therefore, the self-heating of the hot spot is done predominantly by the α particles released from the DT reactions. Detailed numerical simulations as well as analytic estimates have shown that the ρR of the central hot spot must be ~ 0.3 g/cm^2 for efficient self-heating to occur. If the heating rate of the central fuel mass due to $P\,dV$ compression associated with the remaining imploding fuel mass and due to α heating exceeds the cooling rate from radiation and from thermal conduction to the cold surrounding high density fuel, ignition will occur. Once ignition occurs, heating of the surrounding main fuel layer, due predominantly to α particles, results in a radially outward propagating burn wave.

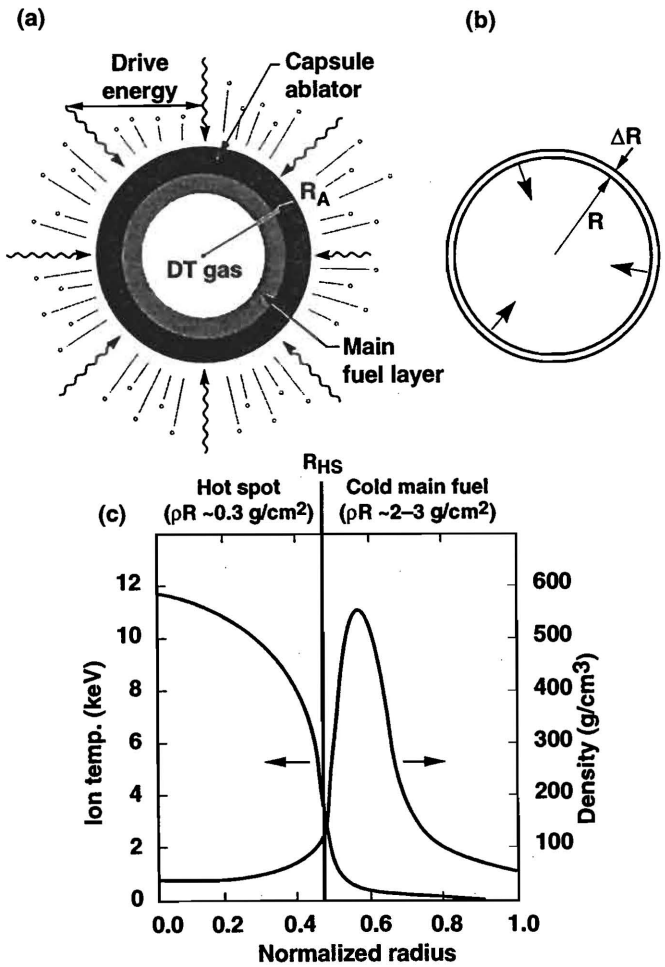

FIG. 2.3. Many high gain ICF capsules have common features. (a) Spherical shell composed of an ablator surrounding a main, cryogenic fuel layer which in turn surrounds an inner DT gas region. (b) During the acceleration phase, the shell compresses to a thickness ΔR *less than its original thickness. Hydrodynamic instabilities limit* R/ΔR. *(c) Fuel temperature and density profile at a time near ignition.* R_{HS} *is the radius of the central hot spot and is usually defined as the position where* $\rho R \approx 0.3$ *g/cm*^{2} *as measured from the origin.*

2.2.4.1. High Gain ICF Capsule Designs

Figure 2.3 shows some common features associated with ICF capsules. High gain ICF capsules are generally spherical shells made up of an outer ablator material (of low to moderate atomic number, Z) that surrounds a thick main fuel layer of DT. This main fuel layer, in turn, surrounds a low density gas region composed of deuterium and tritium (Fig. 2.3(a)). In the implosion process, several features are important. We define the in-flight aspect ratio (IFAR) as the ratio of the shell radius R as it implodes to its thickness ΔR (Fig. 2.3(b)). Hydrodynamic instabilities during the implosion impose limits on this ratio, which results in a minimum pressure or incident driver intensity. This minimum depends on the required implosion velocity, which in turn depends on the capsule size. Typical minimum implosion velocities required for high gain ICF capsules are (3–4) $\times$ 10^7 cm/s. The fuel temperature and density profiles at a time near ignition for a generic high gain ICF capsule are shown in Fig. 2.3(c). The hot spot convergence ratio C_R is defined as the ratio of the initial outer radius of the ablator to the final compressed radius of the hot spot, R_{HS}, at the time of ignition. Asymmetries and instabilities limit the convergence ratio to less than 30–40.

Having briefly introduced the important concepts associated with ICF, in the next section we shall discuss these issues in more detail. Again, we shall limit our discussion to those issues of importance to future high gain capsule designs.

2.3. ICF CAPSULE IMPLOSION PHYSICS

ICF capsule implosions can be achieved using two methods. The first is referred to as direct drive, where the incident laser or charged particle beams directly irradiate the ICF fusion capsule. The second method is referred to as indirect drive, whereby the incident energy associated with the laser or charged particle beams is first absorbed in a high Z enclosure, or hohlraum, which surrounds the capsule. The hohlraum emits X rays which then drive the capsule implosion. Figures 2.4 and 2.5 show the different types of target used for direct and indirect drive implosions, respectively. The capsule is the fuel container and ablator. For direct drive targets, the terms target and capsule are synonymous. For indirect drive, the target includes the capsule and the hohlraum.

Figure 2.4 presents direct drive capsule designs along with their associated driver pulse shapes. The exact capsule dimensions depend upon the driver energy. Typical capsule radii for driver energies of a few megajoules are 2–3 mm. Figure 2.5(a) shows a generic indirect drive laser driven hohlraum target design. Figure 2.5(b) displays a light or heavy ion design with more nearly uniform irradiation in which the incident energy from the ions is deposited within a low density

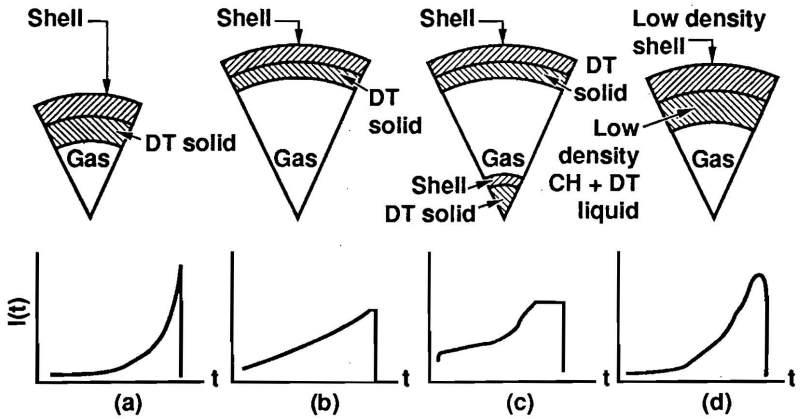

FIG. 2.4. Different direct drive capsule designs and their associated driver pulse shapes: (a) medium aspect ratio (ratio of target radius and shell thickness) target and shaped driver pulse; (b) high aspect ratio target; (c) double-shell target; (d) low ablator density, low aspect ratio target.

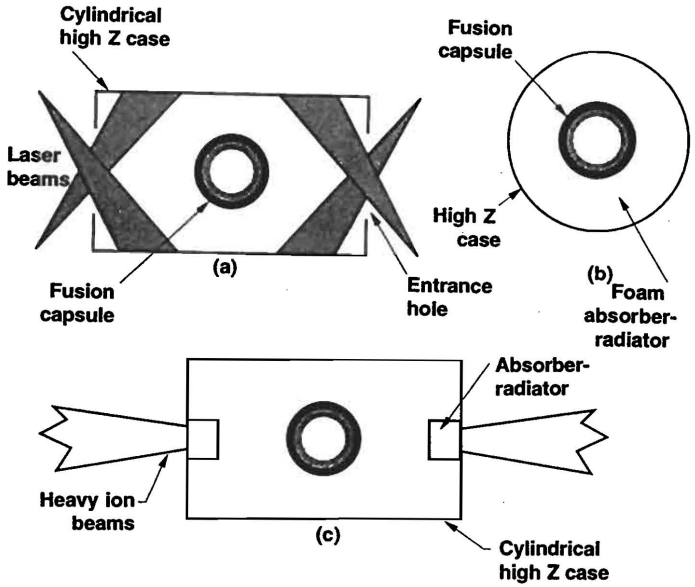

FIG. 2.5. Different indirect drive target designs: (a) laser driven (cylindrical converter); (b) heavy or light ion driven (spherical converter); (c) heavy ion driven (cylindrical converter).

material surrounding the capsule. Figure 2.5(c) is similar to (a) except that the incident energy is delivered in the form of heavy ions and deposited in two cylindrical absorber–radiators (one on either end). Hohlraum dimensions depend upon driver energy. At energies of a few megajoules, high Z (e.g. Pb) hohlraum diameters are 0.5–1.0 cm, lengths are 1–2 cm and thicknesses are a few tens of micrometres.

2.3.1. Equations of State

To understand ICF capsule implosions, knowledge of the behaviour of the capsule material under extreme conditions of density, temperature and pressure is required. Density and temperature of the matter in different parts of the target during an ICF implosion may vary within wide limits: $0 \leq \rho \leq 10^3$ g/cm^3, $0 \leq T \leq 10^2$ keV. Under these conditions information is required not only for the solid, liquid and gaseous states but also for conditions where ionization and radiation processes become important, as well as very high densities where the de Broglie wavelengths become comparable to the interparticle spacing, resulting in quantum effects becoming very important. The published results for Thomas–Fermi–Dirac models [2.13–2.15] for the equations of state, with quantum corrections that take into account partial ionization at low temperatures and densities and degeneration of the electron gas at high density, have been found to agree with experimental data.

2.3.2. Absorption of Driver Energy

2.3.2.1. Absorption: Lasers

There are three basic processes associated with the absorption of laser radiation in high temperature laser produced plasma: inverse bremsstrahlung, resonance absorption and parametric processes.

2.3.2.1.1. INVERSE BREMSSTRAHLUNG ABSORPTION

Inverse bremsstrahlung absorption is a classical absorption process caused by the scattering of the plasma electrons, accelerated in the light wave, on the plasma ions [2.16]. The absorption coefficient (ratio of the absorbed laser energy to the energy of the incident laser radiation) is determined by the frequency of the electron–ion collisions in the underdense plasma corona (the region of the plasma where the plasma frequency (ω_p) is less than or equal to the frequency of the laser wave (ω_L)). (The surface where $\omega_p = \omega_L$ is referred to as the critical surface and the density at that surface (n_{cr}) as the critical density.) The inverse bremsstrahlung coefficient is given by

$$K_{ab} = \frac{\nu_{ei}(n_{cr}) L_h}{c}$$

where

$$\nu_{ei}(n_{cr}) = \frac{4(2\pi)^{1/2} Ze^4 \Lambda_{ei} n_{cr}}{3m_e^{1/2}(kT_e)^{3/2}}$$

is the frequency of the electron–ion collisions; T_e is the temperature of the plasma electrons; Z is the degree of plasma ionization; e and m_e are the charge and mass of the electron, respectively; Λ_{ei} is the Coulomb logarithm ($\Lambda_{ei} \approx 8$–10); $n_{cr} = \omega_L^2 m_e/4\pi e^2$ is the critical density; c is the speed of light; $L_h \approx v\tau_L$ is the scale of the underdense plasma region; v is the plasma velocity; and τ_L is the laser pulse duration.

Detailed analysis of the inverse bremsstrahlung absorption process shows that the absorption efficiency decreases as the laser intensity and wavelength of the laser radiation increase and increases with the duration of the laser pulse. For high gain ICF capsule designs, the laser intensity (I), wavelength (λ_L) and laser pulse duration of interest are $I \geq 5 \times 10^{13}$–1×10^{15} W/cm^2, $\lambda_L \leq 531$ nm and $\tau_L \geq 1$–10 ns. Experimental results and theoretical predictions of absorption under these conditions have shown that the absorption of the incident laser energy is between 70 and 95%.

2.3.2.1.2. RESONANCE ABSORPTION

As the laser intensity and wavelength of the laser radiation increase, the role of other absorption processes can become significant. Resonance absorption is an example of one of these processes [2.17]. Resonance absorption is the transformation of the incident laser electromagnetic wave into electron plasma waves. For example, when plane polarized light (whose electric field E is parallel to the plane of incidence) is obliquely incident on an electron density gradient, electron plasma waves can be driven.

It can be shown that the coefficient of the resonance absorption increases with $I\lambda^2$. The energy flux of the plasma wave (W) is determined by the energy of electron oscillations in the field of the laser wave (E_{os}):

$$W \approx E_{os}(2m_e E_{os})^{1/2} n_{cr}$$

where $E_{os} = I\lambda^2 e^2/4\pi m_e c^3$.

Therefore, the resonance absorption coefficient $K_r \approx W\omega_L/I\omega_p$ is proportional to $(I\lambda^2)^{1/2}$. Controlling resonance absorption is important in ICF capsule implosions owing to the generation of fast electrons. Fast electrons can preheat the fuel, increasing the entropy and therefore preventing Fermi-degenerate compression of the fuel (increasing α, see Section 2.2.4), which results in larger driver energies being required to achieve the same density and ρR conditions. Experimental and

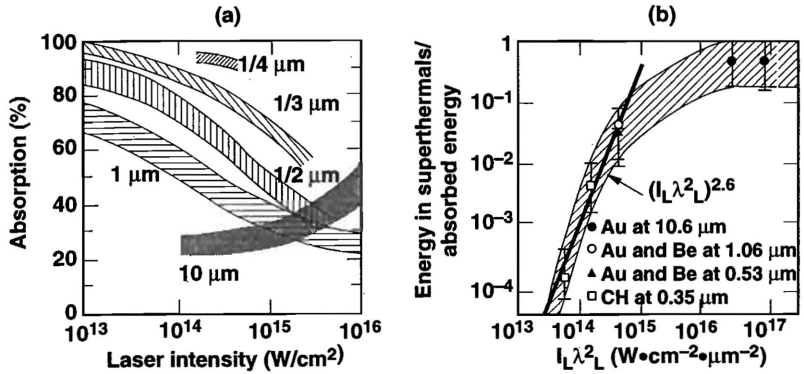

FIG. 2.6. (a) Absorption efficiency versus incident laser intensity (I_L) for various laser irradiation wavelengths (λ_L) and (b) the fractional energy in superthermal electrons versus $I_L\lambda_L^2$ for gold and plastic (CH).

theoretical work has shown that resonance absorption is minimized in the intensity regime of interest for high gain ICF by using laser irradiation wavelengths of less than 531 nm.

Experimental data for the absorption fraction and the amount of energy in superthermal (hot) electrons resulting from resonance absorption are shown in Fig. 2.6. These experimental results are from a number of ICF laboratories throughout the world. The information contained in Fig. 2.6 formed the basis for the ICF community's choice to pursue the use of short wavelength ($\lambda_L \leq 531$ nm) laser irradiation for ICF capsule implosions. From Fig. 2.6(a) it can be seen that for $\lambda_L \leq 531$ nm the absorption efficiency is in excess of 70% for the intensity range of interest to ICF. Figure 2.6(b) shows that for $\lambda_L \leq 531$ nm and the intensity range of interest to ICF the energy associated with superthermal electrons is acceptably small.

2.3.2.1.3. PARAMETRIC PROCESSES

For short wavelength laser irradiation and intensities greater than $\sim 10^{15}$ W/cm^2, plasma collective parametric processes can become significant. This group of processes is caused by the development of decay instabilities in the plasma under the action of the incident electromagnetic wave. The decay instabilities of potential interest to ICF are: stimulated Brillouin scattering (SBS, decay of the incident photon to a reflected photon and a phonon), stimulated Raman scattering

(SRS, decay of the incident photon to a scattered photon and a plasmon), ion acoustic (IA) instability (decay of the incident photon to a plasmon and an ion acoustic wave), and two plasmon decay (TPD, decay of the incident photon into two plasmons).

Parametric instabilities are an amplification of the decay waves caused by feedback between the decay waves and the pumping incidence wave. Therefore, the power of this feedback increases with laser intensity and relative size of the region where the instability is developing compared with the wavelength of pumping radiation.

The SBS process leads to decreased absorption of the incident laser energy. The effect of SRS on absorption is not as straightforward, because this process leads not only to scattering of the laser radiation but also to absorption of the laser radiation as a consequence of electron plasma wave excitation. SRS (and TPD) also has the potential for generating hot electrons. As discussed previously, the generation of hot electrons must be minimized for high gain ICF capsule implosion.

Current high gain capsule designs use the latest experimental and theoretical understanding associated with parametric instabilities so as to avoid their potential effects on capsule implosions. The issues associated with parametric processes in high gain capsule designs represent an area which requires more experimental and theoretical work. Experiments are being carried out in many ICF laboratories to address these issues using techniques to generate plasma conditions relevant to high gain capsule designs.

2.3.2.2. *Absorption: Ion Beams*

Ion beam energy deposition in a plasma is predominantly due to the transfer of energy from the beam ions to the free and bound plasma electrons as a result of collisions between these particles. The physics of ion beam stopping in hot matter is expected to be classical with little modification due to plasma collective processes and electron degeneracy effects. Although no experiments on ion stopping have been done under ICF conditions, recent experiments in hot matter are consistent with theoretical predictions [2.18]. For ICF conditions, absorption efficiencies approaching 100% appear feasible for both light and heavy ions.

2.3.3. Pulse Shaping and Ablation Pressure

As presented in Section 2.2.3, the range of interest for the external driving (ablation) pressure during an ICF capsule implosion is between 10^7 and 10^8 atm (10^{12} and 10^{13} Pa). A number of ICF laboratories throughout the world have experimentally measured the ablation pressure for a variety of laser irradiances and wavelengths. Figure 2.7 displays a number of experimental data sets for ablation pressure versus incident intensity.

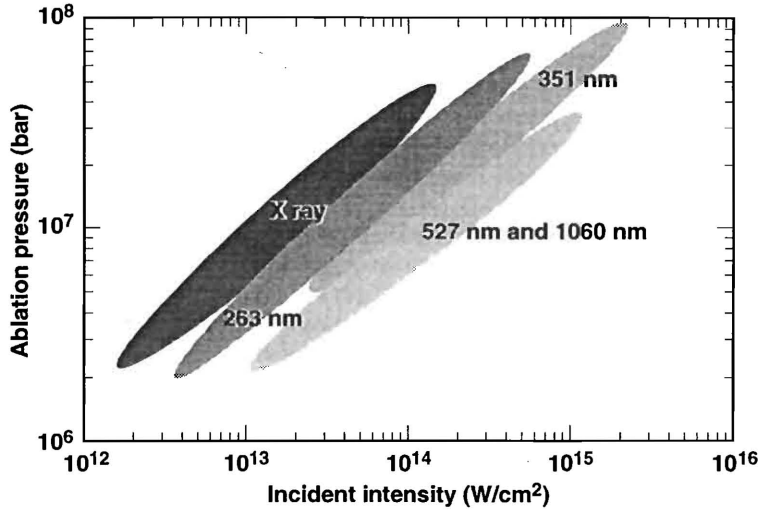

FIG. 2.7. Measured ablation pressure versus incident laser intensity.

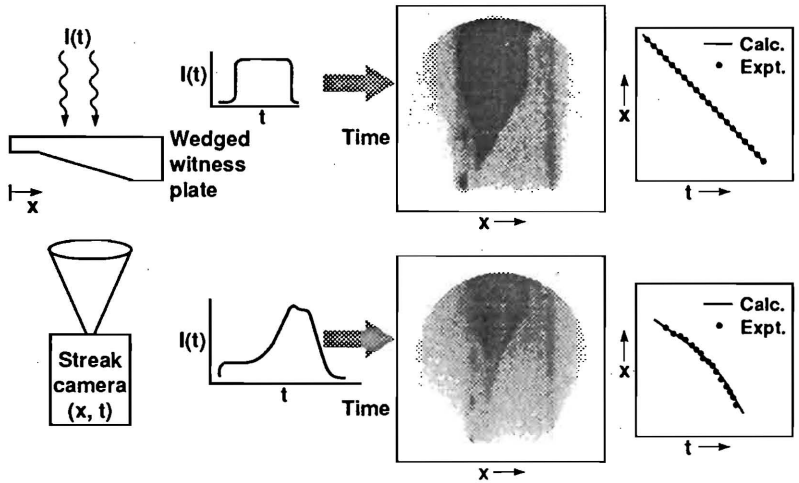

FIG. 2.8. Experimental set-up, measured pulse shapes, streak camera data, and numerical simulation and experimental comparisons of indirectly driven shock wave measurements for square and shaped laser pulses. These experiments demonstrate the ability to produce time varying ablation pressures and that numerical simulations are in good agreement with observed shock trajectories.

Another important technique for controlling the isentrope (entropy levels) of an ICF capsule implosion is to temporally shape the incident driver energy. Figure 2.4 contains some examples of potential pulse shapes used to drive ICF implosions. By tailoring the drive pulse shape in time, the level of preheating associated with shocks can be controlled. Hydrodynamic stability considerations (as well as driver issues) will set the requirements on the pulse shapes that will be used in future high gain ICF capsule designs.

On Nova, a technique for experimentally determining the shock velocity generated by a laser pulse shape has been developed [2.19]. Figure 2.8 shows the experimental set-up, the measured pulse shapes and the shock trajectories for two different pulse shape experiments. Also included are the numerical simulations of the actual experiments. It can be seen from this figure that the numerical simulations are able to accurately predict the resulting time variation in the drive pressure on the witness plate and the shock velocity over a wide range of pulse shapes.

2.3.4. X Ray Production

In the indirect drive approach to ICF, the laser or charged particle beams are first absorbed within a high Z hohlraum, which surrounds the capsule. A significant fraction of the absorbed energy is converted to X rays, which then drive the capsule implosion. For radiation drive to achieve high gain, it is necessary to convert a large fraction of the driver energy into X rays. Both laser and ion beams can achieve high X ray conversion efficiency, but they have opposite intensity scaling. For lasers the conversion efficiency decreases with increasing intensity, while for ion beams it increases. Examples of typical laser driven and heavy ion driven hohlraums are shown in Figs 2.5(a)–(c). The differences between the two types of hohlraum are largely dictated by the differences in beam deposition and X ray production physics for the two types of driver. To produce the ablation pressures mentioned in Section 2.3.3 requires radiation temperatures in the hohlraum of 200–350 eV.

2.3.4.1. Efficiency of X Ray Production: Lasers

When laser light is absorbed on an isolated disc of high Z material such as gold or lead, a significant fraction of the absorbed energy is radiated back as X rays. For intensities of interest to ICF, i.e. 10^{14}–10^{15} W/cm^2, the efficiency of conversion to X rays increases as the laser wavelength and the intensity decrease [2.20]. As described earlier, the laser absorption occurs in material at or below the critical density. At high temperature or long laser wavelength, this absorption generally produces temperatures that are too high in a region that is of too low density for optimal reradiation of the absorbed energy in the form of X rays. Electron conduction must transport the absorbed energy to a higher density and lower temperature region, where most of the X rays are then produced. As the intensity drops, or as

the laser wavelength decreases, the absorption produces more nearly optimal conditions so that losses incurred in the transport process are less and conversion efficiency is higher. It has also been found that the X ray conversion efficiency increases with the length of the laser pulse. Instantaneous conversion efficiencies in excess of 80% are observed for 3–4 ns pulses at an intensity of (3–5) $\times$ 10^{14} W/cm^2.

Both the atomic physics of high Z materials and calculations of electron transport from the absorption region to the emission region pose difficult computational challenges. Hohlraums have added computational complexity owing to the large flux of X rays and the confined plasma produced by ablation of the hohlraum and capsule material due to both the laser beams and X rays. The numerical calculations can predict the trends in intensity, wavelength and pulse length but must generally be normalized to achieve quantitative agreement with experiments. In spite of the complexities, a conversion efficiency of about 70% is characteristic for the bulk of the experiments conducted on facilities such as Nova [2.20], GEKKO XII [2.21, 2.22] and Phebus [2.23].

2.3.4.2. Efficiency of X Ray Production: Ion Beams

A heavy ion driver must concentrate the delivered energy into a geometry such as that shown in Fig. 2.5(b) or (c). This change in hohlraum geometry is required because the X ray conversion process for ions is very different than that for laser heated plasmas. Ion beams are generally absorbed in a relatively low Z material that heats up and then radiates like a black body if the radiator has an optical depth approximately equal to a Planck mean free path. The energy balance equation for an ion beam can be written as

$$I = R\frac{\mathrm{d}C}{\mathrm{d}t} + \frac{\mathrm{d}E_\mathrm{k}}{\mathrm{d}t} + \sigma_\mathrm{r}T^4$$

where R is the ion range (g/cm^2), C is the specific energy of the absorber and E_k is the kinetic energy of expansion of the absorber. The heat capacity term, which is proportional to the temperature T, is the dominant term at low temperature. At high temperature, the radiative term dominates. The kinetic energy term can generally be made small by appropriate choice of absorber material. If the intensity is too low, the absorber material never heats up sufficiently to become an efficient radiator before the pulse ends. At high intensity, the absorber heats up quickly and then radiates very efficiently. The intensity required for efficient conversion increases as the range increases, since the longer range results in a higher heat capacity of the absorber and a longer time before radiation becomes efficient.

Few data currently exist for conversion of ion beam energy into X rays. However, the physics of the radiation process is much less complex than for lasers. Conversion efficiencies of 60–80% appear feasible in calculations.

2.3.5. Irradiation Uniformity

High gain ICF capsule implosions require a high degree of uniformity of irradiation of the capsule by the incident laser beams or X rays. Detailed numerical simulations have shown that the non-uniformity of irradiation must be less than ~1% RMS. The actual modal spectrum of irradiation non-uniformity that can contain this 1% RMS is dependent on the particular capsule design and method of implosion (direct versus indirect) being considered. For the direct drive approach the number, deposition and quality of each laser beam must be optimized. Owing to the nature of the indirect drive approach, individual beam quality may be relaxed; however, the number of beams and placement must still be accurately controlled.

2.3.5.1. Direct Drive: Lasers

In direct drive, the sources of irradiation non-uniformity have been identified [2.24, 2.25]. These sources are: the finite number and placement of individual beams about the capsule, beam and/or capsule misalignment, beam misfocus, power and/or energy imbalance between individual beams, and intensity non-uniformities associated with individual beam radial profiles. The same studies have also shown that the effects of these non-uniformities can be divided into two broad categories with respect to the wavelength of the resulting non-uniformity on the capsule. The individual beam radial profiles result in predominantly short wavelength ($l \geq 10$, where l is the Legendre mode number) modes of irradiation non-uniformity, while all the remaining sources result in long wavelength ($l < 10$) modes.

The thermal smoothing in the corona is able to partly smooth out non-uniformities of energy deposition, owing to lateral heat diffusion between the critical and ablation surfaces. For direct drive the energy deposited in the vicinity of the critical surface is transported to the ablation region (the ablation surface is the location where the acceleration changes sign) predominantly by electron thermal conduction. For the conditions found in the ablated region, the electron thermal conductivity (κ_e) has a strong dependence on the electron temperature, $\kappa_e \propto T_e^{5/2}$. In planar geometry, the smoothing of defects in the irradiation pattern is described by the 'cloudy day' model [2.26]; the attenuation is $\exp(-k_m D)$, where D is the distance between the ablation and critical surfaces and k_m is the wavenumber of the perturbation being considered. The larger the distance D or the shorter the wavelength of the non-uniformity, the more efficient the smoothing. Fluctuations in the ablation pressure resulting from non-uniform laser irradiation can be reduced by increasing D. The distance D can be increased by increasing the wavelength of the laser radiation and/or the laser intensity. However, these options can adversely affect both the entropy of the imploding fuel, owing to hot electron production by resonance absorption and parametric processes, and the hydrodynamic efficiency of the implosion, owing to the lower absorption efficiency as the laser wavelength and intensity are

increased and to the reduced transport efficiency between the absorption region and the ablation front. (The hydrodynamic efficiency is defined as the total kinetic energy of the imploding capsule material divided by the driver energy absorbed.)

The first step in optimizing the irradiation uniformity on a direct drive capsule is to determine the placement of individual beams about the capsule. Figure 2.9 presents the results of such an optimization. The graph, calculated assuming 'perfect' parabolic individual beam profiles, shows that the RMS amplitude of the irradiation uniformity can be reduced to values less than 1% for as few as ~20 beams. However, as a direct drive capsule implodes, the critical surface moves radially inward. The focus ratio (Fig. 2.9) therefore increases from 1 to ~1.8 during the laser pulse for a high gain direct drive capsule design. Taking these factors into account and neglecting any potential effects of irradiation smoothing by the plasma results in a direct drive system requiring ~60 beams to ensure adequate uniformity in long wavelength modes throughout the implosion. Studies have also shown that the other sources of long wavelength irradiation non-uniformity can be controlled with proper attention to the design of the laser system. The exact requirements with

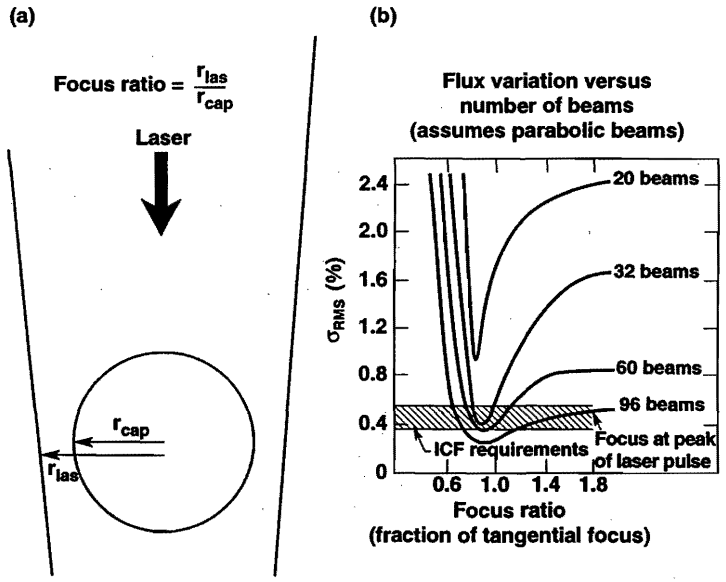

FIG. 2.9. A large number of beams are required to obtain adequate symmetry for direct drive capsules in the absence of electron conduction smoothing in the plasma.

regard to these issues depend on the capsule design under consideration. (Future experiments will examine the amount of uniformity required in long wavelength modes for direct drive ICF capsule implosions. This information, coupled with experimental results for the amount of thermal smoothing that takes place for longer wavelength modes, may lead to a reduction in the number of laser beams required for direct drive laser systems.)

The irregularities in the energy distribution in the focal spot, which are a consequence of phase and amplitude errors in the laser beam, result in short wavelength irradiation non-uniformities [2.27]. These short wavelength modes, the amplitude and phase of which vary during the ablation process, are potentially the most dangerous as they can seed the Rayleigh–Taylor instability. Several techniques have been proposed, and experimentally implemented, to improve the quality of individual laser beams (see Chapter 3 for details). It is yet to be demonstrated that the required beam smoothness, particularly at early times, can be obtained.

2.3.5.2. *Indirect Drive: Lasers*

Embedding the capsule in a black body radiation field, generated through the use of a hohlraum, potentially relaxes the requirement on the quality of an individual laser beam. In addition, X ray driven ablation has a higher ablation velocity (velocity at which material is ablated from the imploding shell) than direct drive and therefore has a lower development of hydrodynamic instabilities (Section 2.3.6).

Owing to the multiple radiative exchanges involving thermal radiation, illumination non-uniformities at high spatial frequencies conveyed by the laser beams are reduced in a hohlraum environment. Lower order mode non-uniformities due to long wavelength variations in the X ray emission (differences in emission from directly heated regions and laser entrance holes, for example) are not efficiently attenuated.

In order to achieve control of symmetry (long wavelength modes) for indirect drive implosions, it is necessary to have reproducible beam propagation conditions in the hohlraum. These conditions must be consistent with accurate placement of the laser beams and plasma parametric instabilities such as SRS and SBS, which can cause redirection of energy in the hohlraum. Numerical studies have shown that these parametric processes must be kept below the 5–10% level.

2.3.5.3. *Indirect Drive: Heavy Ion Beams*

For ion beam driven implosions, while direct drive has been studied, indirect drive is considered more likely to achieve the symmetry requirements. As in the laser X ray driven option, it involves a high Z case enclosing the target (Fig. 2.5). The main difference between this type of target and an indirectly driven laser target is a consequence of the ion–plasma interaction physics. Theoretical predictions have found that 1–2% RMS irradiation uniformity could be achieved in a heavy ion indirectly driven target.

2.3.6. Symmetry and Hydrodynamic Stability

As shown in Section 2.2, high gain ICF capsule implosions require final DT fuel densities in the range 100–1000 g/cm^3. During the implosion small non-uniformities at the ablation surface can be amplified through a number of processes. The two most important are perturbations, which grow in proportion to t^2 (acceleration variations, for example), and growth due to the Rayleigh–Taylor instability.

2.3.6.1. *Secular* (t^2) *Distortions*

A simple dynamics argument can be used to estimate the acceleration uniformity required for a given capsule implosion. The acceleration uniformity $\delta a/\bar{a}$,

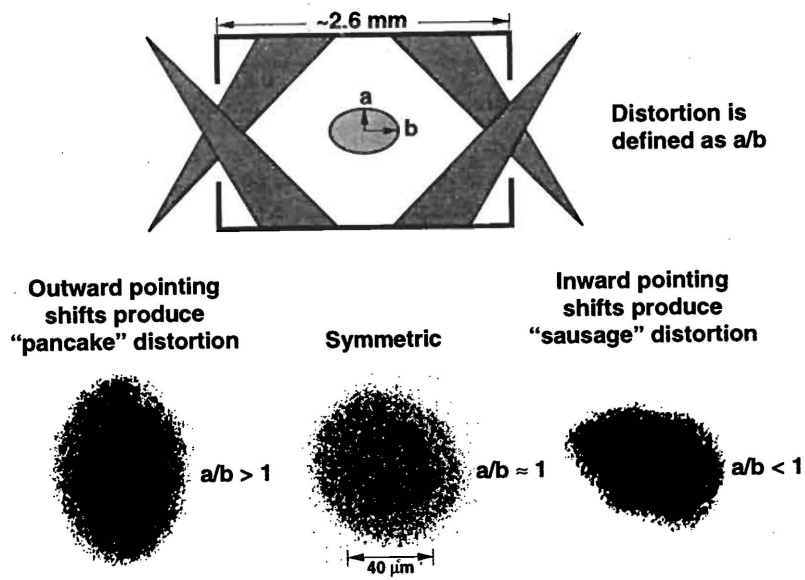

FIG. 2.10. Time integrated images of indirect drive implosion experiment performed at LLNL on a target containing fuel doped with a high Z gas. By varying the hohlraum geometry, it is possible to change the shape of the imploded core. The diagram at the top shows a generic hohlraum target used for these experiments along with the definition of distortion (a/b). *By changing the location of the beams, the shape of the core is changed from elliptical (left) to nearly circular (centre). The measured degree of non-sphericity of the nearly circular imploded core implies (from calculations) a drive uniformity better than 3%, which is close to adequate for high gain targets.*

regard to these issues depend on the capsule design under consideration. (Future experiments will examine the amount of uniformity required in long wavelength modes for direct drive ICF capsule implosions. This information, coupled with experimental results for the amount of thermal smoothing that takes place for longer wavelength modes, may lead to a reduction in the number of laser beams required for direct drive laser systems.)

The irregularities in the energy distribution in the focal spot, which are a consequence of phase and amplitude errors in the laser beam, result in short wavelength irradiation non-uniformities [2.27]. These short wavelength modes, the amplitude and phase of which vary during the ablation process, are potentially the most dangerous as they can seed the Rayleigh–Taylor instability. Several techniques have been proposed, and experimentally implemented, to improve the quality of individual laser beams (see Chapter 3 for details). It is yet to be demonstrated that the required beam smoothness, particularly at early times, can be obtained.

2.3.5.2. *Indirect Drive: Lasers*

Embedding the capsule in a black body radiation field, generated through the use of a hohlraum, potentially relaxes the requirement on the quality of an individual laser beam. In addition, X ray driven ablation has a higher ablation velocity (velocity at which material is ablated from the imploding shell) than direct drive and therefore has a lower development of hydrodynamic instabilities (Section 2.3.6).

Owing to the multiple radiative exchanges involving thermal radiation, illumination non-uniformities at high spatial frequencies conveyed by the laser beams are reduced in a hohlraum environment. Lower order mode non-uniformities due to long wavelength variations in the X ray emission (differences in emission from directly heated regions and laser entrance holes, for example) are not efficiently attenuated.

In order to achieve control of symmetry (long wavelength modes) for indirect drive implosions, it is necessary to have reproducible beam propagation conditions in the hohlraum. These conditions must be consistent with accurate placement of the laser beams and plasma parametric instabilities such as SRS and SBS, which can cause redirection of energy in the hohlraum. Numerical studies have shown that these parametric processes must be kept below the 5–10% level.

2.3.5.3. *Indirect Drive: Heavy Ion Beams*

For ion beam driven implosions, while direct drive has been studied, indirect drive is considered more likely to achieve the symmetry requirements. As in the laser X ray driven option, it involves a high Z case enclosing the target (Fig. 2.5). The main difference between this type of target and an indirectly driven laser target is a consequence of the ion–plasma interaction physics. Theoretical predictions have found that 1–2% RMS irradiation uniformity could be achieved in a heavy ion indirectly driven target.

2.3.6. Symmetry and Hydrodynamic Stability

As shown in Section 2.2, high gain ICF capsule implosions require final DT fuel densities in the range 100–1000 g/cm^3. During the implosion small non-uniformities at the ablation surface can be amplified through a number of processes. The two most important are perturbations, which grow in proportion to t^2 (acceleration variations, for example), and growth due to the Rayleigh–Taylor instability.

2.3.6.1. *Secular (t^2) Distortions*

A simple dynamics argument can be used to estimate the acceleration uniformity required for a given capsule implosion. The acceleration uniformity $\delta a/\bar{a}$,

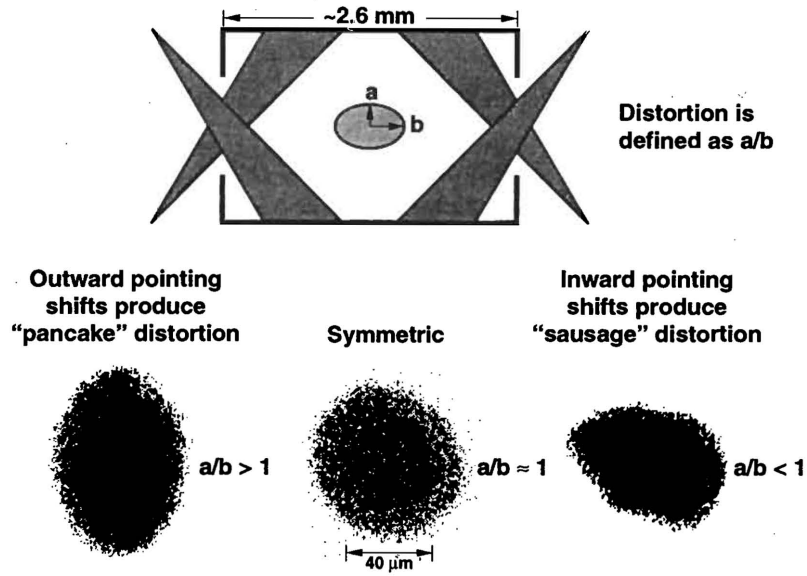

FIG. 2.10. Time integrated images of indirect drive implosion experiment performed at LLNL on a target containing fuel doped with a high Z gas. By varying the hohlraum geometry, it is possible to change the shape of the imploded core. The diagram at the top shows a generic hohlraum target used for these experiments along with the definition of distortion (a/b). By changing the location of the beams, the shape of the core is changed from elliptical (left) to nearly circular (centre). The measured degree of non-sphericity of the nearly circular imploded core implies (from calculations) a drive uniformity better than 3%, which is close to adequate for high gain targets.

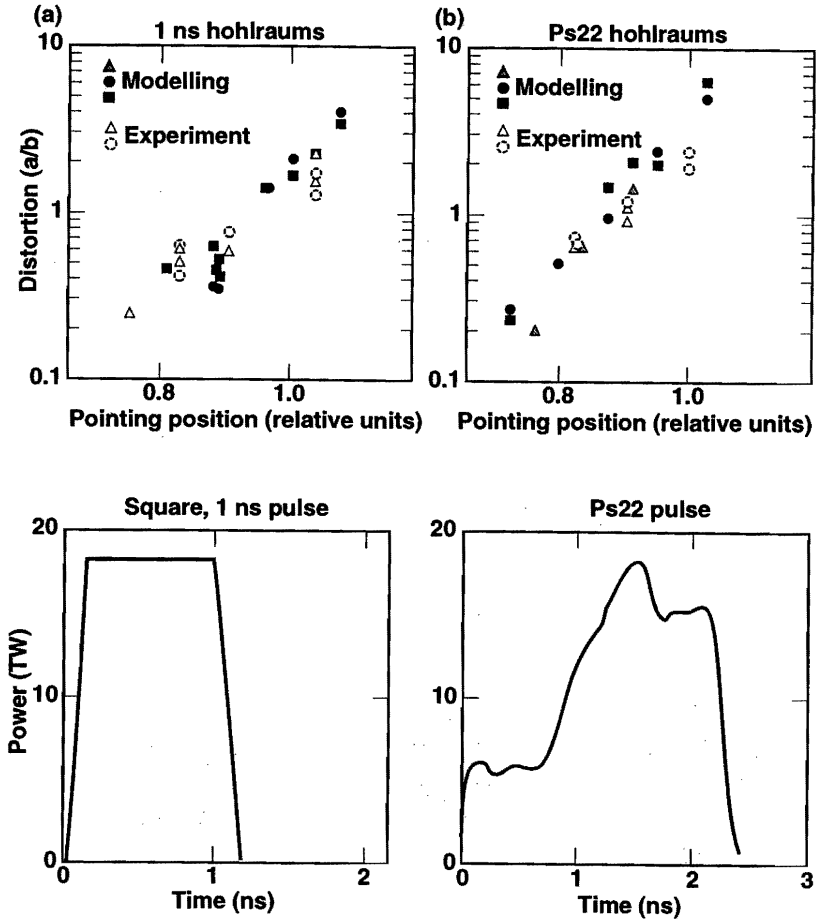

FIG. 2.11. Measured and simulated final core distortions versus pointing position for indirect drive capsule implosion experiments conducted on Nova using two different laser pulse shapes. Pulse shape 22 (Ps22) is as specified in the lower right hand figure.

where δa and $\bar{a}$ are the azimuthal acceleration perturbation and average acceleration, respectively, is given by

$$\frac{\delta a}{\bar{a}} = \frac{\delta R}{\bar{R}} \frac{1}{C_R - 1}$$

where $\delta R/\bar{R}$ is the final hot spot distortion and C_R is the hot spot convergence ratio.

For high gain ICF capsule implosions, typical values of C_R needed for ignition are in the range 20–40. If the requirement of central hot spot formation and ignition is $\delta R \leq \frac{1}{2}R$ this corresponds to having to achieve a uniformity of acceleration of 1–2%. How the acceleration uniformity relates to the uniformity required in the ablation pressure depends on the method used to implode the capsule (direct versus indirect) and the particular capsule design. In general, of course, the greater the uniformity achievable, the greater the convergence ratio allowable.

Experiments on Nova [2.19] have shown that flux uniformity (and subsequent drive (pressure) uniformity) to within a few per cent can be achieved inside hohlraums. This uniformity was demonstrated by imaging the compressed fuel region of an X ray driven implosion. A typical target used in these experiments consists of a plastic shell filled with DD fuel and argon trace gas. The fuel is imaged using both a 100 ps X ray framing camera and a time integrated X ray pinhole camera.

By varying either the hohlraum geometry or the laser focusing, the symmetry of the imploded fuel can be controlled [2.19, 2.28, 2.29]. Implosions can be obtained that have more flux along the axis of the hohlraum or along the midplane of the hohlraum, as shown by the left and right hand images in Fig. 2.10. In the experiments in Fig. 2.10, the laser beams were pointed to different locations inside a 2.6 mm long hohlraum by changing the pointing angle: 45°, 51° and 54°, from left to right in the figure. With the appropriate choice of geometry or pointing, it is possible to achieve fluxes uniform to within a few per cent, as shown in the centre image of Fig. 2.10. The images in Fig. 2.10 give a time averaged measure of flux uniformity. These types of experiment have been conducted for a variety of laser pulse shapes. Figure 2.11 shows experimental results compared with a two dimensional numerical simulation obtained at LLNL for distortion versus pointing position using two different laser pulse shapes (the associated pulse shapes are shown below the respective figures).

2.3.6.2. Rayleigh–Taylor Instability: Linear Stage

High gain ICF capsules are designed so as to limit the development of hydrodynamic instabilities to the linear or weakly non-linear regime. Under these circumstances, theoretical models and numerical simulations indicate that the thickness of the perturbed or unstable (mixed) region between the hot spot and the surrounding main fuel layer near the time of ignition is given by the RMS sum of the

SECTION 3: Pgs. 56- 63

Experiments have also been conducted to determine the compressed fuel density obtained during the implosion process. Experiments conducted on GEKKO XII using 531 nm direct drive irradiation of DT doped plastic shells (with no gas fill) have achieved densities in the plastic of 200–600 g/cm^3 (Fig. 2.19) [2.45]. Direct drive experiments conducted on Omega using 351 nm irradiation of cryogenic DT fuel surrounded by glass ablators achieved average fuel densities in the range 20–40 g/cm^3 [2.47]. Both of these high density implosion experiments produced neutron yields significantly lower than predicted for an ideal spherical implosion. This degradation has been attributed to the effects of hydrodynamic instability seeded by irradiation non-uniformities and capsule fabrication defects. Data from all participating laboratories have indicated reductions in final core performance similar to those presented above. It is clear that understanding hydrodynamic instabilities and secular distortions in imploding capsules is an important area of research in the ICF community.

2.3.7. Capsule Ignition and Burn

Conditions for fuel ignition may be obtained from the analysis of the energy balance for the compressed DT fuel [2.48–2.50]:

$$3\frac{\rho}{m_i}\frac{dT}{dt} = -P\nabla u + \nabla K_e \nabla T - W_R + W_\alpha \tag{2.3}$$

where $T_e = T_i = T$, and ρ, m_i, P and u are the density, ion mass (2.5 times proton mass), pressure and flow velocity. In Eq. (2.3) the first term of the right hand side represents the pressure–volume work associated with compression and expansion, the second term electron cooling via conduction, the third term radiation cooling and the last term α particle heating.

In assuming the DT fuel to be compressed with homogeneous core radius R and density ρ, each term on the right hand side of Eq. (2.3) can be approximately evaluated as follows:

— Expansion loss $$W_E \approx 2\frac{\rho T}{m_i}\frac{3}{R}2c_s \tag{2.4}$$

— Conduction loss $$W_C \approx k_0 T^{7/2}\frac{1}{R^2} \tag{2.5}$$

— Radiation loss $$W_R \approx A_0 \rho^2 T^{1/2} \tag{2.6}$$

Equation (2.5) assumes that $dR/dt = 2c_s$ and uses the relations $u = -\rho\, d\rho/dt$ and $\rho \approx R^{-3}$ (the confinement time is given to be $t = R/4c_s$). In Eqs (2.5) and (2.6), k_0 and A_0 are constants. The α particle heating term can be expressed in the form

$$W_\alpha = \left(\frac{\rho}{2m_i}\right)^2 \langle\overline{\sigma v}\rangle_{DT} f_\alpha \epsilon_\alpha \tag{2.7}$$

where $\epsilon_\alpha = 3.52$ MeV and f_α is a heating rate determined by the stopping power of the α particles. In the case where the electron temperature is lower than ~30 keV, stopping by electrons is dominant compared with the ions and the ions are heated indirectly through the electron–ion energy relaxation process. The density dependence of $\rho\lambda_\alpha$, where λ_α is the stopping range of α particles, is sufficiently weak and can be given approximately by

$$\rho\lambda_\alpha = 0.04\, T_e^{3/2}\ (\mathrm{g/cm^2}) \tag{2.8}$$

where T_e is the temperature (keV). By considering the α particles generated at the centre, the heating rate is given in the form

$$f_\alpha = \begin{cases} 1 - (1 - \rho R/\rho\lambda_\alpha)^2 & (R < \lambda_\alpha) \\ 1 & (R > \lambda_\alpha) \end{cases} \tag{2.9}$$

Assuming the balance $W_E + W_C + W_R = W_\alpha$ and using relations (2.4)–(2.9), the following equation is obtained:

$$8.7 \times 10^{18} T^{7/2} + 1.27 \times 10^{23} T^{3/2}\rho R + 2.77 \times 10^{23} T^{1/2}(\rho R)^2 = 8.07 \times 10^{40}\langle\overline{\sigma v}\rangle \zeta_\alpha (\rho R)^2 \tag{2.10}$$

where ζ_α is the fraction of the α energy deposited in a radius R. Since $\langle\overline{\sigma v}\rangle$ is a function of T, Eq. (2.10) provides a relation between ρR and T. When we assume $\zeta_\alpha = 1$, Eq. (2.10) becomes a quadratic equation in ρR for a given T and it is found that there is a critical T for which Eq. (2.10) has a solution. This can be seen by balancing W_R and W_α, requiring real values of ρR and T, and satisfying the relation

$$\langle\overline{\sigma v}\rangle \geq 3.43 \times 10^{-18} T^{1/2}$$

By using data on $\langle\overline{\sigma v}\rangle$ (Fig. 2.1), we conclude that T should be larger than 4.4 keV for DT fuel.

In Fig. 2.20, the solution of Eq. (2.10) is plotted as the thick solid line. From this figure it is found that the minimum ρR for fuel ignition is approximately

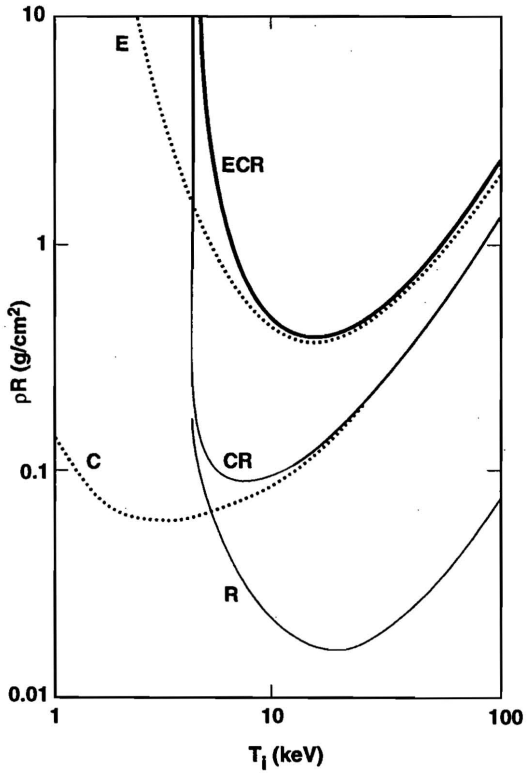

FIG. 2.20. Ignition condition given by balancing α particle heating against cooling due to expansion, radiation and electron heat conduction [2.50]. The conduction is plotted as a thick solid line (ECR). For comparison, a balance relation defined by $W_C + W_R = W_\alpha$ *is plotted as a thin solid line (CR); another relation* $W_E = W_\alpha$ *by a dotted line (E),* $W_C = W_\alpha$ *by a dotted line (C) and* $W_R = W_\alpha$ *by a solid line (R).*

$\rho R = 0.4$ g/cm^2 near $T = 10$ keV. In a more general form it can be concluded that as a minimum

$$(\rho R)^3 T \geq 0.1\text{–}0.5$$

is required for substantial fuel ignition.

Figure 2.20 also shows a balance relation defined by $W_C + W_R = W_\alpha$ (neglecting the expansion loss) (thin solid line (CR)), along with the relations $W_E = W_\alpha$ (dotted line (E)), $W_C = W_\alpha$ (dotted line (C)) and $W_R = W_\alpha$ (solid line (R)). From the figure it is seen that in the range $T < 4$ keV radiation cooling is significant, but in the range $T > 5$ keV expansion is the dominant loss mechanism.

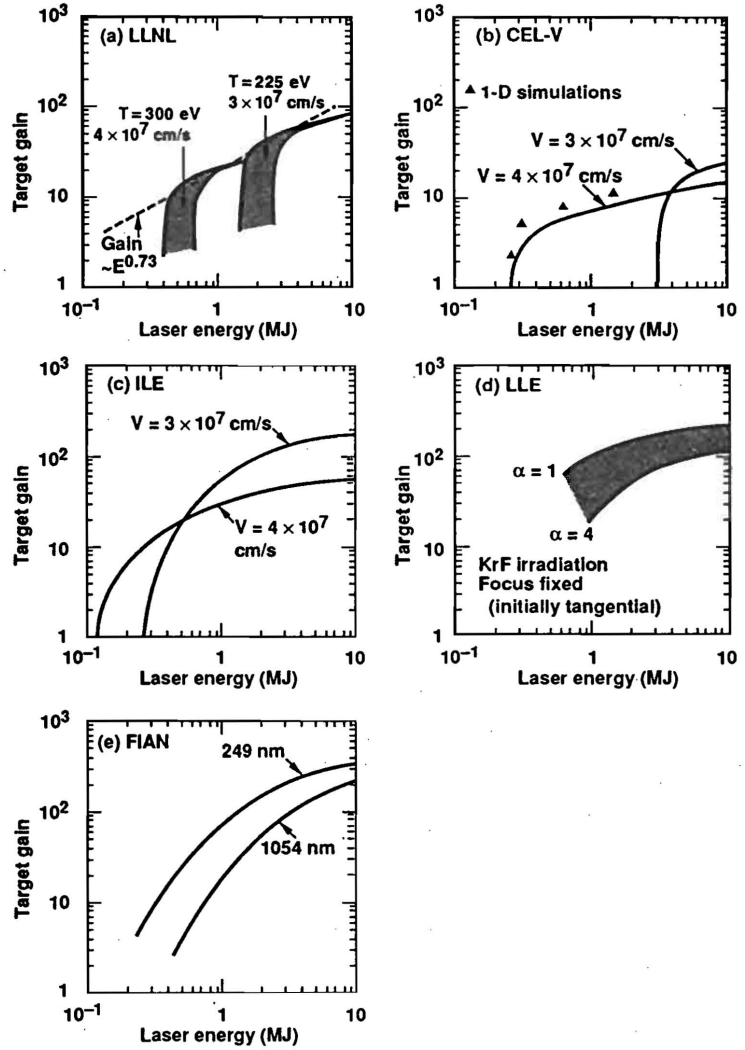

FIG. 2.21. Numerical predictions of thermonuclear gain versus incident laser energy for (a, b) indirect and (c–e) direct drive laser capsule implosions. (a) LLNL gain predictions for 351 nm laser driver and two implosion velocities. (b) CEL-V gain predictions for 351 nm laser driver and two implosion velocities. (c) ILE gain predictions for 351 nm laser driver. (d) LLE gain predictions for 249 nm laser driver. The upper boundary of the region displayed corresponds to Fermi-degenerate (α = 1) implosions and the lower boundary to α = 4 implosions. (e) FIAN gain predictions for 249 nm and 1054 nm laser drivers.

2.3.8. Thermonuclear Gain

One and two dimensional numerical simulation codes are used to calculate gains for capsules at the incident energy levels for IFE reactors ($E_d \geq 1$ MJ). These simulation codes include complex mathematical models which include algorithms for computing all of the most important processes associated with ICF implosions. These codes are based on solving the equations of hydrodynamics with electron and ion heat conductivities, viscosity, energy sources due to incident energy deposition and fusion reaction products, and various energy transfer mechanisms, including radiation and fast electrons. Numerical calculations of the gain performance of ICF capsule implosions have been carried out by many laboratories: LLNL, Los Alamos National Laboratory (LANL) and LLE in the USA, the P.N. Lebedev Physics Institute (FIAN), the Institute for Mathematical Modelling (IMM), the Russian Institute for Experimental Physics (VNIIEF) and the Russian Institute for Technical Physics (VNIITF) in the Russian Federation, ILE in Japan, CEL-V in France and the Instituto de Fusión Nuclear (DENIM) in Spain.

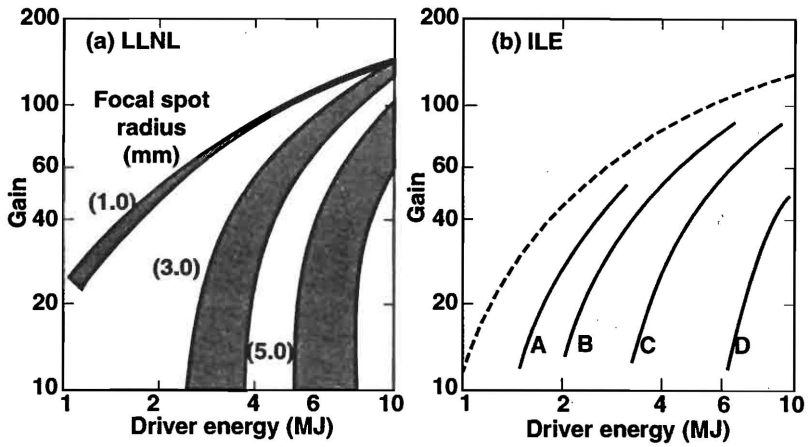

FIG. 2.22. Numerical predictions of thermonuclear gain versus incident heavy ion driver energy for indirect drive capsule implosions. (a) LLNL simulations for ion ranges of 0.05 and 0.1 g/cm^2 (top and bottom of grey bands, respectively) and for the spot radii identified (1.0–5.0 mm). (b) ILE calculated gain curves for indirect drive heavy ion fusion targets as a function of driver energy. The solid curves are model results corresponding to a pressure of 0.2 Tbar (2 × 10^{16} Pa), an isentrope parameter of 3.5 and different values of $r^{3/2}R$ *= 0.005 (A), 0.01 (B), 0.02 (C) and 0.04 (D), where* r *is the radius of a cylindrical X ray converter (cm) and* R *is the stopping range of the ion beam (g/cm^2). The broken line corresponds to an ideal converter with 100% efficiency.*

Figures 2.21 and 2.22 display the target gain predictions for laser driven and ion driven ICF capsule implosions, respectively, as computed by a number of ICF laboratories throughout the world. Figures 2.21(a) and (b) represent indirect drive predictions from LLNL [2.51] and CEL-V [2.52], respectively. Figures 2.21(c), (d) and (e) show the results of direct drive simulations from ILE [2.53], LLE [2.51, 2.54], and FIAN [2.55], respectively.

Each laboratory has computed its gain curves independently using its best theoretical modelling and understanding of experimental results to date. The physics used and the degree of optimism about the outcome of important physics issues introduced in this chapter play an important role in the generation of these curves. For example, the curves in Fig. 2.21(a) are all calculated under the assumption of a fixed hohlraum coupling efficiency of 15% (i.e. 15% of the laser energy is ultimately absorbed by the capsule as X rays). The right hand band corresponds to a radiation temperature of 225 eV, the left to 300 eV. As can be seen, ignition can be achieved at lower driver energy by operating at a higher hohlraum temperature, but LLNL currently believes that laser–plasma interactions inside ICF hohlraums with capsules will limit the temperatures to less than 325–350 eV, and therefore implosion velocities will be limited to less than about 4.5 × 10^7 cm/s. A temperature of 300 eV has been achieved in Nova experiments. The width of each shaded band corresponds to the uncertainty in the achievable capsule surface finish. The far left hand edge corresponds to the gain achievable for perfectly uniform implosions. The right hand edge of the band corresponds to the gain for targets with surface non-uniformities of 50–100 nm. Capsules with such surface finishes are used in ICF experiments today.

As the driver energy increases, the minimum implosion velocity required to ignite a capsule decreases. If the minimum velocity at any driver size is exceeded, the capsule will still ignite. However, there is a performance penalty for operating above the minimum velocity. The gain will drop because less mass will implode and there will be less yield for a given energy. Hence, the optimum strategy implies operation at the minimum implosion velocity consistent with the desired yield or driver size. For a fixed capsule surface finish, this optimum is given by the dashed line through the two curves in Fig. 2.21(a). This line approximately follows the scaling given by the relation $G \approx E_d^{3/4}$.

When the capsules are limited to a similar degree of hydrodynamic instability, detailed numerical calculations by LLE (and LLNL) predict comparable gains for laser driven direct drive capsule implosions, as shown in Fig. 2.21(d). The higher coupling efficiency of direct drive essentially balances the greater sensitivity to hydrodynamic instability.

All of these calculations assume that both direct and indirect drive will be able to produce adequate implosion symmetry. Gains for indirect drive can be a factor of 2 or more above those of Fig. 2.21(a) if the hohlraum coupling efficiency can be improved, and direct drive gains can be a factor of 2 or more higher if the

hydrodynamic instability constraints are relaxed by improvements in capsule fabrication techniques and irradiation uniformity.

Results of LLNL simulations [2.56] and ILE calculations [2.57] for gains using heavy ion drivers are shown in Figs 2.22(a) and (b), respectively. In Fig. 2.22(a) the capsules used for the heavy ion target gain curves are the same as those assumed in the laser driven indirect drive targets, and the hohlraums are similar to those shown in Fig. 2.5(c). The coupling of ion beam energy to absorbed capsule energy is simply recalculated. The capsule implosion velocities are varied with capsule size in the same way as for the laser driven indirect drive targets discussed above. The heavy ion target gains are sensitive to the ion range and the focal spot size. This sensitivity arises from the energy required to heat the material in the X ray converters to a temperature at which the converter material will radiate efficiently. As the ion range or spot size is reduced, less mass is heated. Because of this, as the ion range is reduced, calculations predict a higher gain for a given spot size or a larger tolerable spot size for a given gain.

The optimal choice of focal spot size and ion range is largely an accelerator issue since targets with adequate gain are feasible for a wide selection of values of these parameters. In the target designs with larger spot size, lower intensity and shorter range, the accelerator must be able to transport more current, and the focusing system must be able to focus more current or the beams must be partially charge neutralized. Target designs using ions with a range of about 0.1 g/cm^2 and a spot size of 2.5–3.0 mm radius are the current baseline heavy ion designs because the longer range ions, which have lower beam current for a given driver energy, can be ballistically focused without current or charge neutralization. This method of focusing is well understood theoretically and provides heavy ion target point designs with a high confidence focusing approach. This is viewed as important because of the present lack of data to conclusively support the feasibility of charge neutralization schemes for focusing (Section 3.4).

This situation could change because of work being done in the US light ion programme. Beams being produced by the pulsed power machines used in this programme are inherently high current and must rely on current and charge neutralized focusing schemes. The theoretical understanding being developed in the light ion programme, and the experiments currently being carried out and planned, can provide the information required to base heavy ion designs on neutralized focusing schemes. To within a factor of ~ 2, SNL predictions for light ion gain results are in agreement with those shown in Fig. 2.22(a). As shown in Fig. 2.22(a), higher gain can be achieved, particularly for smaller driver sizes, if spot sizes of 1 mm radius can be achieved. If spot sizes of no smaller than 5 mm radius can be obtained, high gain is still possible but the minimum driver size increases by about a factor of 2.

There continues to be an interest in determining the minimum driver energy to ignite an ICF capsule. As presently understood, ignition at lower driver energies

can theoretically be achieved by increasing the implosion velocity. The present understanding associated with laser driven hohlraum physics and hydrodynamic stability constraints indicates that $\sim 4 \times 10^7$ cm/s is the maximum implosion velocity that can be achieved for laser driven indirect drive capsule implosions. Therefore, as shown in Figs 2.21(a) and (b), approximately 500–600 kJ of laser energy would be required to ignite an indirectly driven capsule implosion. Similar studies have been performed for laser driven direct drive capsule implosions. These studies have shown that for implosion velocities limited by plasma physics constraints, approximately 200–500 kJ of laser energy would be required to ignite a direct drive capsule implosion (Figs 2.21(c)–(e)). It is important to note, however, that at these smaller energies both directly and indirectly driven capsule implosion would require a much more optimistic outcome associated with the effects of hydrodynamic instabilities on capsule implosions than presently assumed possible. Additionally, the studies show that these designs represent capsules at the limits of performance and therefore would have little margin for error.

2.4. ADVANCED FUSION FUELS

As previously stated, considering the values of $\langle \overline{\sigma v} \rangle$ in the temperature range of interest, the first IFE reactor designs will be based on a DT fuel cycle. However, properties of some of the other fusion reactions (Fig. 2.1) are of interest for future reactor systems since the reaction products involve predominantly charged particles and not neutrons. It has been suggested that this offers the potential of minimizing radioactivity and shielding issues associated with IFE power plants.

There are two important issues that make the use of advanced fusion fuels of marginal interest to IFE power plants. The first is that the internal blanket in many IFE reactor designs moderates and absorbs the 14 MeV neutrons produced by the DT reaction and thereby reduces the activation and damage to structural materials automatically (Section 3.4). The only advantage of the advanced fuel systems, then, would be the reduced tritium inventory. While some of the other fusion reactions being considered do not require tritium, they all will produce some, at least in secondary reactions. Furthermore, the ignition temperatures (and consequently the required driver energy) are much higher than for DT. Therefore, an IFE target using advanced fuels would probably be designed with a small core (called the spark plug) region of DT so that ignition can take place at lower temperatures. Therefore, some tritium would be present in any event. However, the tritium inventory with advanced fuels will be much smaller than with DT. The second, and perhaps more important, issue is that the temperatures and fuel areal densities required for efficient burnup of these advanced fusion fuels are much higher than for DT. Advanced fuel ICF would require a much larger laser system than for a DT cycle or a more optimistic outcome associated with symmetry and stability issues than presently believed possible. Therefore, this book will concentrate on the DT cycle.

2.5. CONCLUSION

This chapter has covered the various physical processes that take place during an ICF capsule implosion. These processes ultimately define the reliability of the prediction of the thermonuclear yield for future ICF high gain capsule designs at a given driver energy.

The understanding of the physics of ICF hohlraums and capsule implosions has made significant progress over recent years. These advances have been due to substantial improvements in experimental diagnostics and the quality of the laser drivers used to conduct the experiments as well as improved theoretical models. One method to measure the advances made in recent ICF experiments is to show the results in terms of a Lawson plot. The results from ICF experiments conducted around the world are shown in Fig. 2.23. Target gains of 10^{-3} have already been achieved.

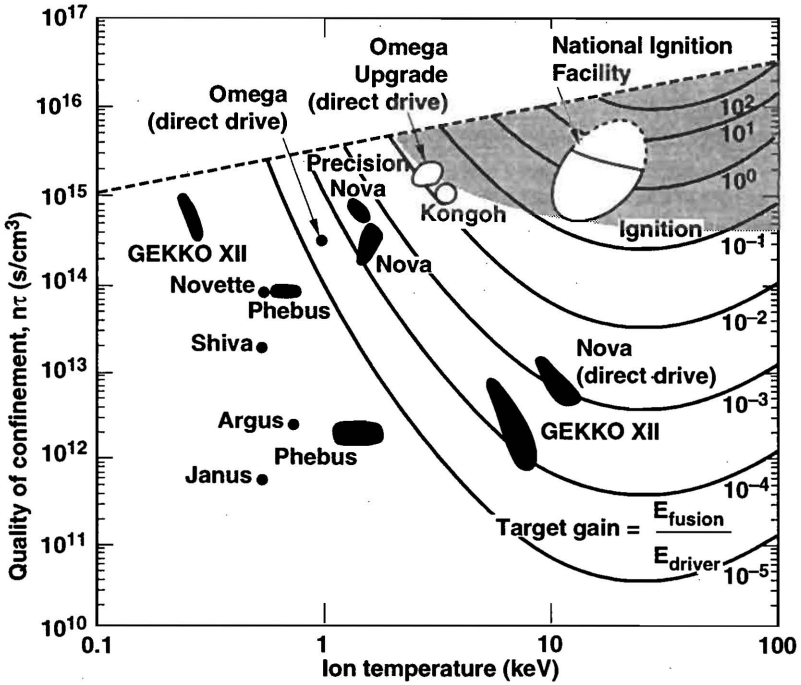

FIG. 2.23. Recent progress in ICF research as measured using the product nτ as a function of the central ion temperature. Also included in this figure are projections for the Omega Upgrade laser system (LLE), presently under construction, and the proposed US National Ignition Facility. Several machines have experimented with two or more distinctly different target configurations. These are shown in the figure as separate areas for the same machine.

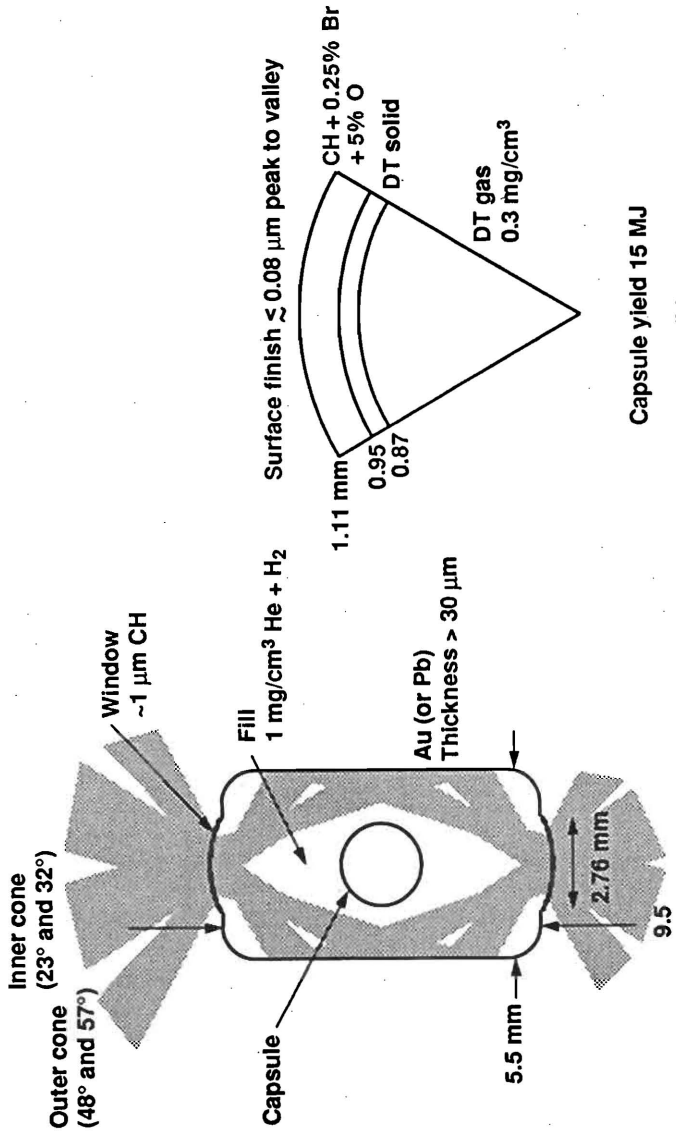

FIG. 2.24. Current proposed target design for achieving ignition and modest gain on the NIF. (a) Hohlraum design: 'outer' cones enter at 48° and 57° with a 500 mm best focus at entrance hole, f/8; 'inner' cones enter at 23° and 32° with a 500 mm best focus at ~ 3 mm inside the hohlraum, f/8. All laser beams are assumed to be azimuthally symmetric. (b) Capsule design.

The ICF programme will continue to use experimental data from ongoing laboratory experiments for both direct and indirect drive capsule implosions to refine the theoretical understanding of the important processes associated with ICF capsule implosions. It is generally agreed within the world ICF community that the next important step for ICF is the demonstration of ignition and propagating burn in the laboratory. The US ICF programme has this as its next major goal (to demonstrate ignition in the laboratory using a glass laser driver). Previous indirect drive experiments conducted on Nova and results from H/C form the basis for that decision. At the time this book was being drafted, the conceptual design for the proposed US facility, referred to as the National Ignition Facility (NIF), had just been completed. This facility would have a solid state laser capable of delivering 1.8 MJ of 351 nm wavelength laser energy to the target using 192 square (40 cm on a side) beams. For indirect drive targets, the beams will be arranged in four axisymmetric cones, two coming in from the top of the chamber and two from the bottom. (Chapter 5 contains a more complete description.) The indirect drive target design under consideration for achieving ignition and modest gain in the NIF is shown in Fig. 2.24. The cones coming in from the top and those coming in from the bottom are distinguished as 'inner' and 'outer' cones, respectively, and will be used to provide better control of symmetry during the implosion. The capsule in Fig. 2.24(b) is a cryogenic fuel design with a polythene ablator doped with oxygen and bromine. This indirect drive target is expected to ignite and give a gain of 1–10 with a drive temperature of 300 eV. The NIF can be reconfigured to do experiments with direct drive targets either by adding a second target area or by reconfiguring the beams within the indirect drive target area. A review of LLNL's past and near term experimental and theoretical results is being used in determining whether the US programme proceeds along this path in the near future and builds the NIF.

The demonstration of ignition and burn propagation in the laboratory would complete the basic capsule physics objectives of the ICF programme. Such a demonstration would set the stage for high confidence development of IFE.

References to Chapter 2

[2.1] BASOV, N.G., KROKHIN, O.N., Conditions for heating up of a plasma by the radiation from an optical generator, Sov. Phys. — JETP **19** (1964) 123.

[2.2] NUCKOLLS, J., WOOD, L., THIESSEN, A., ZIMMERMAN, G., Laser compression of matter to super-high densities: Thermonuclear (TN) applications, Nature (London) **239** (1972) 139.

[2.3] Review of the Department of Energy's Inertial Confinement Fusion Program, Final Report, Natl Academy Press, Washington, DC (1990).

[2.4] AFANASIEV, Yu.V., et al., Pis'ma Zh. Ehksp. Teor. Fiz. **21** (1975) 150.

[2.5] NAKAI, S., Inertial confinement, Nucl. Fusion **30** (1990) 1779.

[2.6] LINDL, J.D., "Progress and prospects for indirect drive inertial confinement fusion", Plasma Physics and Controlled Nuclear Fusion Research 1992 (Proc. 14th Int. Conf. Würzburg, 1992), Vol. 3, IAEA, Vienna (1993) 125.

[2.7] CEL-V LASER RESEARCH GROUP, Twenty-two years of laser–matter work at Centre d'études de Limeil-Valenton (CEL-V), Nucl. Fusion **25** (1985) 1333.

[2.8] VELARDE, G., RONEN, Y., MARTINEZ-VAL, J. (Eds), Nuclear Fusion by Inertial Confinement: A Comprehensive Treatise, CRC Press, Boca Raton, FL (1993).

[2.9] FRALEY, G.S., LINNEBUR, E.J., MASON, R.J., MORSE, R.L., Thermonuclear burn characteristics of compressed deuterium–tritium microspheres, Phys. Fluids **17** (1974) 474.

[2.10] LAWSON, J.D., Some criteria for a power producing thermonuclear reactor, Proc. Phys. Soc. London, Sect. B **70** (1957) 6.

[2.11] BODNER, S.E., Critical elements of high gain laser fusion, J. Fusion Energy **1** (1981) 221.

[2.12] TAYLOR, G., Proc. R. Soc. London, Ser. A Math. Phys. Sci. **201** (1950) 192.

[2.13] ZEL'DOVICH, Y.B., RAIZER, Y.P., Physics of Shock Waves and High Temperature Hydrodynamic Phenomena, Academic Press, New York (1966).

[2.14] LATTER, R., Temperature behavior of the Thomas–Fermi statistical model for atoms, Phys. Rev. **99** (1955) 1854.

[2.15] FEYNMAN, R.P., METROPOLIS, N., TELLER, E., Equations of state of elements based on the generalized Fermi–Thomas theory, Phys. Rev. **75** (1949) 1561.

[2.16] JOHNSTON, T.W., DAWSON, J.M., Correct values for high frequency power absorption by inverse bremsstrahlung in plasmas, Phys. Fluids **16** (1973) 722.

[2.17] GINZBURG, V.L., The Propagation of Electromagnetic Waves in Plasmas, Pergamon Press, New York (1964).

[2.18] HOFFMANN, D.H.H., et al., Energy loss of heavy ions in a plasma target, Phys. Rev., A Gen. Phys. **42** (1990) 2313.

[2.19] CAMPBELL, E.M., Recent results from the NOVA program at LLNL, Laser Part. Beams **9** (1991) 209.

[2.20] KAUFFMAN, R.L., X-Ray Conversion Efficiency, 1986 LLNL Laser Program Unclassified Annual Report, UCRL-50021-86, Lawrence Livermore Natl Lab., CA (1986).

[2.21] NISHIMURA, H., et al., X-ray emission and transport in gold plasmas generated by 351 nm laser irradiation, Phys. Rev., A Gen. Phys. **43** (1990) 3073.

[2.22] NISHIMURA, H., et al., X-ray confinement in a gold cavity heated by 351 nm laser light, Phys. Rev., A Gen. Phys. **44** (1991) 8323.

[2.23] JURASZEK, D., et al., Observation of soft X ray emission in the corona of 0.35 μm laser irradiated gold disks, J. Appl. Phys. **70** (1991) 1980.

[2.24] SKUPSKY, S., LEE, K., Uniformity of energy deposition for laser driven fusion, J. Appl. Phys. **54** (1983) 3662.

[2.25] MURAKAMI, M., NISHIHARA, K., AZECHI, H., Irradiation nonuniformity due to imperfections of laser beams, J. Appl. Phys. **74** (1993) 802.

[2.26] BODNER, S.E., Critical elements of high gain laser fusion, J. Fusion Energy **1** (1981) 221.

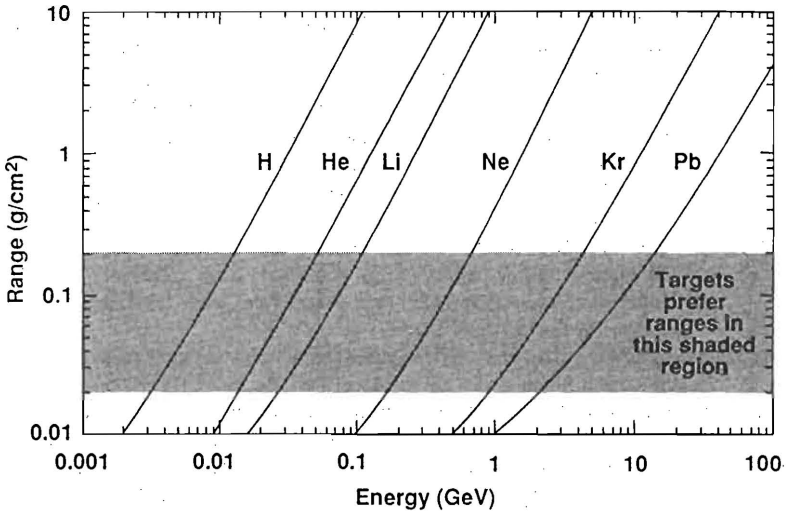

FIG. 3.2.4.1. Ion range in hot material as a function of kinetic energy for a variety of ions. The range appropriate for inertial fusion is about 0.02–0.2 g/cm². This range allows ion kinetic energies on the order of 10 GeV for the heavier ions.

final optic problem

an accelerator can be focused by magnetic fields. The conductors that produce the fields can be shielded from the neutrons, X rays and debris produced by the target. Thus, it may be possible to build a robust, durable focusing system to direct the beams towards the target. The long life and high pulse rate of accelerators are attractive features for the development of fusion energy in that a single driver could be used for a number of development facilities. In summary, high energy accelerator technology is, in many ways, well suited to IFE power production. However, there is one critical requirement that has not been demonstrated, namely the high peak power of several hundred terawatts. Since accelerators, from a technical standpoint, can readily deliver high kinetic energy, high power is really a new requirement on beam current. This requirement pushes accelerators into a hitherto unexplored regime of beam physics and leads to significant departures from standard accelerator design. Nevertheless, much of the technology that has been developed for other applications remains applicable for IFE. The accelerator considerations specifically relevant to IFE power plants will now be discussed.

why not direct?

To drive an ICF target, the ions from an accelerator must have the correct penetration depth. Target calculations show that the penetration depth, or ion range, in terms of areal density should be between about 0.02 and 0.2 g/cm² in order to heat properly the radiating material in an indirect drive target (Fig. 2.5). This constraint on ion range has important consequences for accelerator design. The range

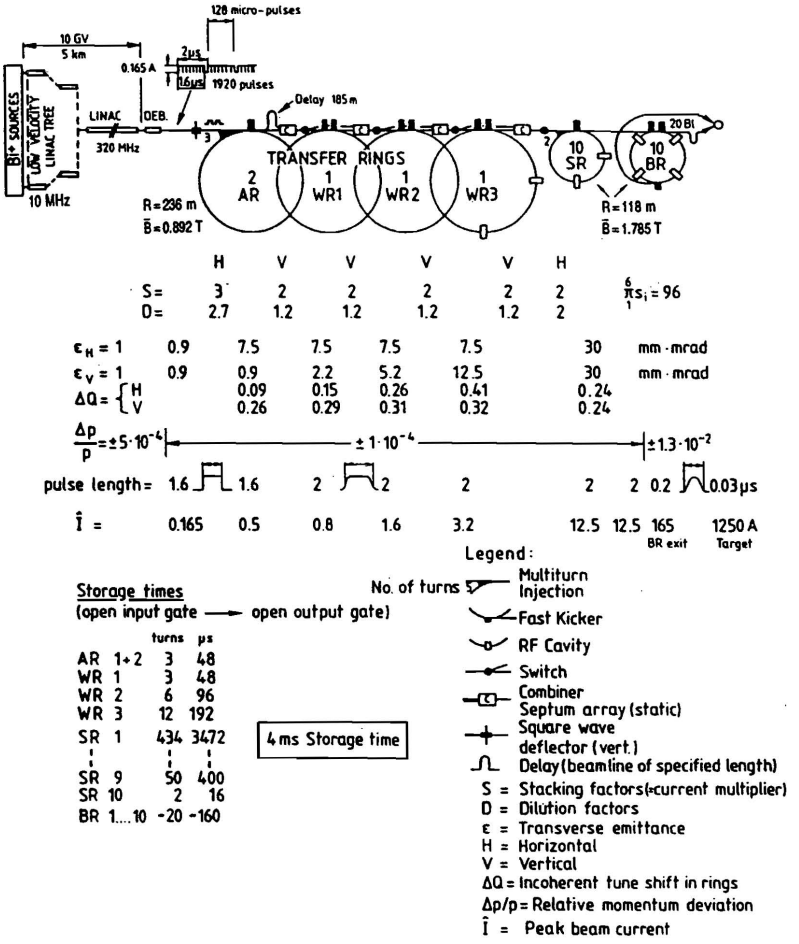

FIG. 3.2.4.5. HIBALL driver concept.

TABLE 3.3.1. SOME REQUIREMENTS OF TARGET PRODUCTION AND POSITIONING

Production rate	5–10 Hz
Production at 70% duty factor	$(1–2) \times 10^8$ targets/year
Polymer shell	
Outer diameter	5.5–6.0 mm
Thickness	300–500 μm
DT fuel per target	2.5–5.0 mg
DT fuel layer thickness	200–300 μm
Capsule roundness defect	$\leq 1\%$
Capsule non-concentricity	$\leq 1\%$
Accuracy of layer thicknesses	0.1 μm
Surface roughness goal, plastic or fuel layers	≤ 100 nm
Accuracy of beam placement from capsule centre	
Direct drive laser	20–30 μm
Indirect drive heavy ion beam	40–60 μm
Hohlraum dimensions	
Diameter	0.5–1.0 cm
Thickness of high Z material	~ 30 μm

is absorbed by the fuel capsule, driving the implosion. The fuel capsule is held in the centre of the hohlraum by a sandwich of thin polymer films (called tenting) or by a very low density foam. Hohlraums driven by lasers have laser entrance holes to admit the focused laser beams; hohlraums driven by ions are fully enclosed because the ion energy can be deposited inside through the hohlraum wall. The thickness of the hohlraum wall is not critical, but the wall must be thick enough to stay together and contain the radiation during the implosion, and as thin as possible to minimize the recycling of activated heavy metal.

The requirements or restrictions placed on the manufacture and positioning of these targets are determined both by target physics constraints to ensure high gain, and by the system performance and economics of the reactor. These are summarized in Table 3.3.1. Since there is no one universally accepted target design, because there are a wide range of acceptable yield–pulse rate combinations that require different target sizes, we give a representative range of acceptable parameter values.

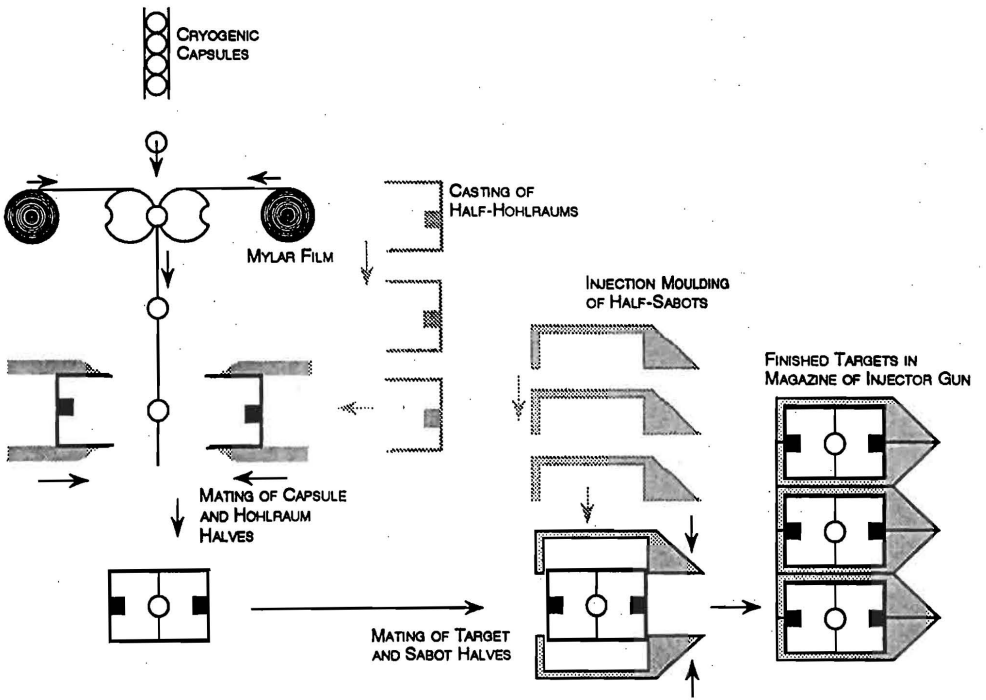

FIG. 3.3.4. Schematic of the automated hohlraum assembly process.

is bonded to an HT-9 ferritic steel tube containing liquid lithium. At a surface energy flux of ~10 J/cm^2 of X rays and debris, there is no vaporization of the first wall. However, condensation of target material on the first wall may require periodic cleaning to prevent a detrimental buildup. Other reactor designs, such as Saturn [3.4.3], the dry wall design by Lawrence Livermore National Laboratory [3.4.6] and the hybrid [3.4.11], are also representative of the dry wall approach.

The use of a cavity fill gas to reduce the high power flux to the structural wall was first pioneered in Solase [3.4.8]. The function of the gas (~1 torr (130 Pa)) is to absorb the X ray and charged particle energy which is emitted in a short burst and reradiate it over a much longer time period. One example of this approach is shown in Fig. 3.4.10, from the SIRIUS-P study [3.4.38]. This is similar to the route taken by previous SIRIUS designs [3.4.24] and the Sombrero reactor [3.4.31].

An example of the wetted wall approach is shown in Fig. 3.4.11, from the wetted wall concept developed by Los Alamos National Laboratory [3.4.2]. A thin film of liquid metal is allowed to coat the first wall and absorb the kinetic energy of the target debris as well as a large fraction of the X ray energy. The liquid metal then

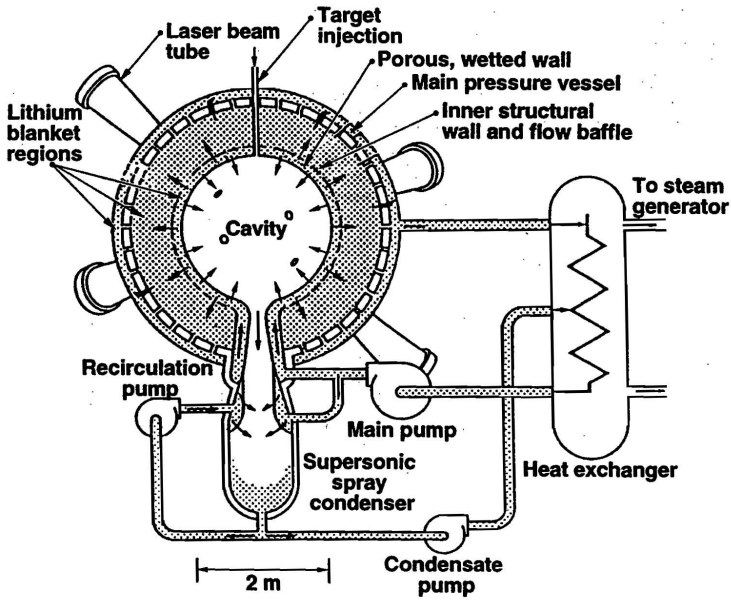

FIG. 3.4.11. The lithium wetted wall concept utilizes a thin, renewable layer of liquid lithium on the metallic first wall to absorb the target debris and photons [3.4.2].

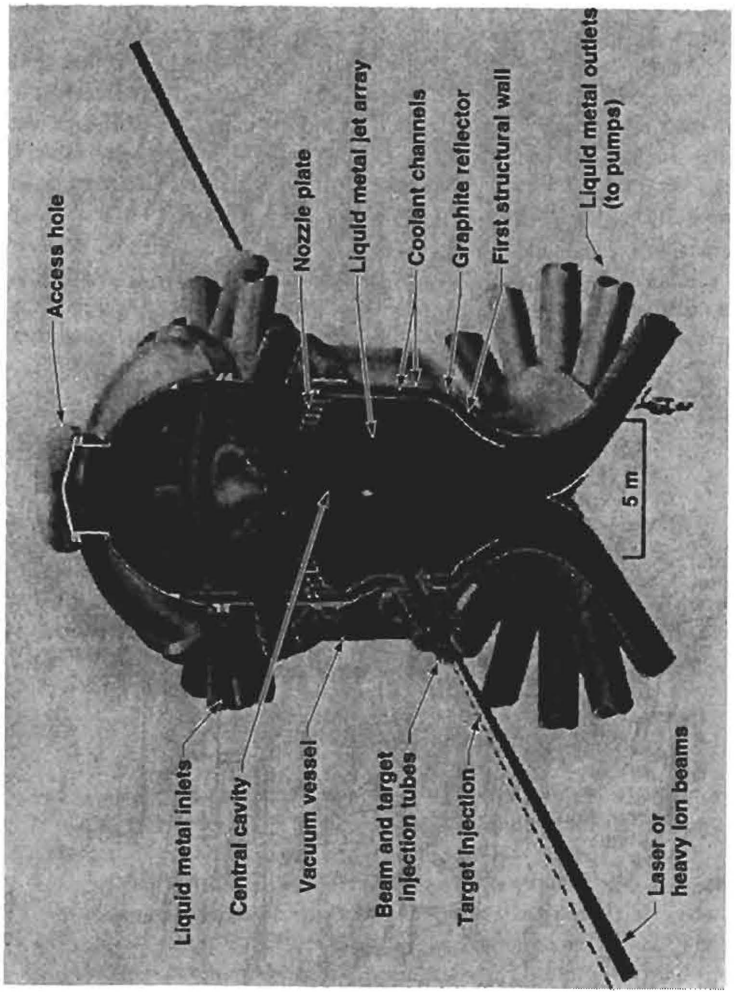

FIG. 3.4.12. The HYLIFE [3.4.12] reactor uses a free-falling stream of liquid metal to absorb the target debris and moderate the neutron spectra. This reactor concept was based on indirect drive of targets with two sided illumination.

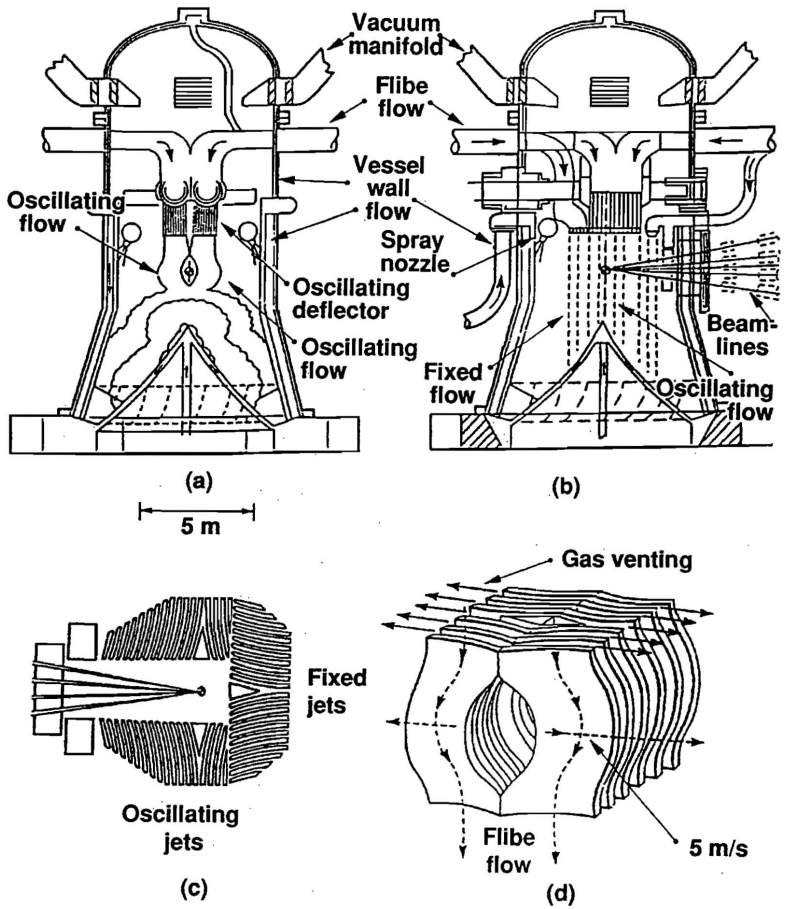

FIG. 3.4.13. The (a) front and (b) side views of the HYLIFE-II [3.4.30] reaction chamber show how indirect drive can be used to ignite an ion target from either one side or two sides. The (c) top and (d) side views of the Flibe flow channels show how neutron attenuation can be achieved while still allowing gas to vent rapidly through the space between the slabs of liquid metal. Flibe flow velocity is 12 m/s.

absorbs the extremely high heat fluxes in a small volume as latent heat. The evaporated material fills the cavity and is pumped out to condense outside the reaction zone. One of the problems with this design is the shock impulse imparted to the first wall by the evaporating liquid metal.

The use of a thick liquid metal stream to protect the structural wall from neutrons was first proposed by Burke [3.4.55] at Argonne National Laboratory. This was followed by the BAM (boiler and moderator) concept from Brookhaven National Laboratory [3.4.9]. However, the most detailed analysis of this concept was done in the HYLIFE study which started in 1979 [3.4.12] (Fig. 3.4.12) and continues in

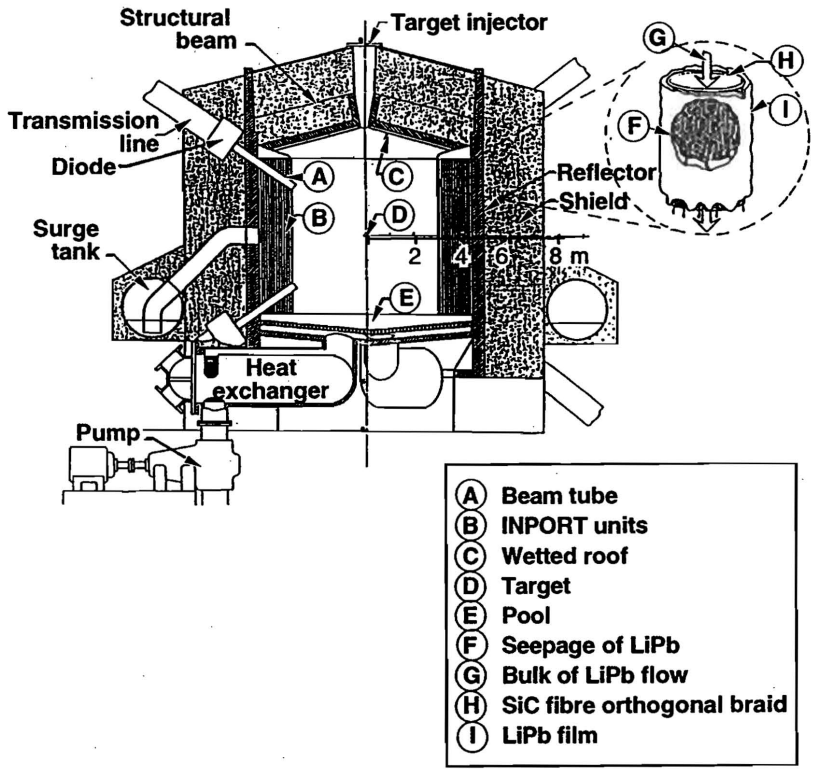

FIG. 3.4.14. The containment of liquid metal in INPORT units allows the coolant to absorb the energy of several pulses during its transit in the reaction chamber of LIBRA [3.4.28]. The wetted surface on the outside of the INPORT unit (shown in the circular inset) mitigates the erosion and shock phenomena associated with dry solid walls.